Small

NANO · MICRO small
www.small-journal.com

RESEARCH ARTICLE

Editor's Choice

Silk Ionomer-Based Modular Nanocoatings for Potential Immuno-Regenerative Cell Therapy in Osteoarthritis

Nilotpal Majumder[1,2] | Parth Jain[2] | Udathari Kumarasinghe[3] | Shangyuan Cui[2] | Evan C. Marcet[2] | Chunmei Li[2] | Cristian Staii[3] | Neeraj Sakhrani[4] | Clark T. Hung[4] | Jugal Kishore Sahoo[2] | Ying Chen[2] | Sourabh Ghosh[1] | David L. Kaplan[2]

[1]Department of Textile and Fibre Engineering, Indian Institute of Technology Delhi, New Delhi, India | [2]Department of Biomedical Engineering, Tufts University, Medford, Massachusetts, USA | [3]Department of Physics and Astronomy, Tufts University, Medford, Massachusetts, USA | [4]Department of Biomedical Engineering, Columbia University, New York, New York, USA

Correspondence: Jugal Kishore Sahoo (jugal.sahoo@tufts.edu) | Ying Chen (ying.chen@tufts.edu) | Sourabh Ghosh (sourabh.ghosh@textile.iitd.ac.in) | David L. Kaplan (david.kaplan@tufts.edu)

Received: 22 December 2025 | **Revised:** 31 March 2026 | **Accepted:** 7 May 2026

Keywords: cell therapy | immunomodulation | immunotherapy | inflammation | nanocoating | osteoarthritis | silk ionomers

ABSTRACT

Silk protein ionomer-based layer-by-layer (LBL) nanocoating strategy was utilized to preserve the viability, metabolic activity and differentiation potential of human mesenchymal stem cells (hMSCs) in an in vitro inflamed osteoarthritis (OA) tissue niche. These temporary ionomer coatings for cell protection were functionalized with cytokines to impart immune-modulatory behavior. The cytokine-functionalized ionomer nanocoatings polarized neutral M0 macrophages into M1 and M2 subtypes, depending on the specific cytokine used, thereby reducing synovial inflammation in an in vitro setup. This approach would potentially abrogate the need for ex vivo polarization before transplantation during immunotherapy. The modular nature of these silk ionomer nanocoatings in tailoring cell surface stability was further validated by extending the cell coatings to 3D spheroids and also by introducing tyramine to the cationic silk ionomer to facilitate covalent crosslinking in addition to the electrostatic interactions between the cell surface and the ionomers. These results demonstrate the versatile and modular nature of silk-based ionomer cell nanocoatings, allowing control at material, cellular, and spheroid levels to tune coating stability and inflammatory responses. These systems uniquely impart immunomodulatory function, providing a biomaterial platform for cell-based immune-regenerative therapy, such as for OA and other inflammatory diseases.

1 | Introduction

Regenerative cell therapies have evolved as a promising approach for managing degenerative and inflammatory disorders, fostering tissue regeneration [1]. Evidently, with persistent limitations in palliative treatment modalities for managing severely degraded and inflammatory conditions like osteoarthritis (OA), cell-guided tissue reconstruction approaches are an essential alternative for the functional restoration of articular cartilage tissue while immunoregulating the peripheral inflammatory niche [2, 3]. These limitations have encouraged researchers to explore stem cell- or immune cell-based therapeutic options for regenerating lost cartilage and attenuating the progressive inflammation in OA. MSCs have an innate advantage of a rapid proliferation rate, a higher tendency for chondrogenic differentiation than adipose-derived stem cells (ADSCs) and articular chondrocytes, and inherent immunomodulatory properties [4, 5] making them important candidates for treating focal cartilage lesions with single-dose intra-articular injections using 10 million/mL cells [6]. However, the limited cell viability and

the inclination toward hypertrophic differentiation under the influence of the inflammatory and oxidative joint microenvironment remain issues [6, 7]. In the context of immunotherapy, recent studies have demonstrated the use of genetically engineered M2-polarized macrophages in promoting cartilage tissue homeostasis while reducing inflammation [8]. Thus, if directly transplanted, the neutral M0 macrophages require an additional step for ex vivo polarization to the M2 phenotype before transplantation, either by exogenous cytokine supplementation [9] or genetic modification techniques [8], making the procedure cumbersome. Furthermore, if the monocytes or M0 macrophages are directly delivered to an inflammatory OA niche, they polarize to the inflammatory M1 phenotype [10], further contributing to the OA pathophysiology by amplifying the inflammatory niche. Therefore, when designing a cellular therapy platform targeted at the osteoarthritic environment, transplanted cells must possess an additional protective layer around their cell membrane to shield the cells from the detrimental joint microenvironment while maintaining cellular integrity and regulating the surrounding immunological niche to initiate healing.

Biomaterial-based cell surface coating strategies have been employed as a protective shield for mammalian cells against various mechanical, biological, and microenvironmental stressors [11–13]. In this direction, we have demonstrated the structural stability of silk-based nanocoatings through layer-by-layer deposition for up to 48 h (maximum), beyond which the nanocoating disengages from the cell surface [14, 15]. Although nanoencapsulation preserved cell viability, the proliferation potential of the L929 murine fibroblasts [14] and the differentiation ability of the THP-1 monocytes [15, 16] and human intestinal organoids [17], the efficacy of the nanocoatings as cell armour against severe environmental and biomechanical stressors akin to the in vivo conditions remains to be determined. Additionally, the direct use of monocytes for cell therapy poses a significant challenge due to their relatively short lifespan in circulation [18]. Further, the requirement for an additional intermediate polarization state before differentiation into their respective M1 or M2 phenotypes for transplantation is an additional complication [19]. Therefore, a comprehensive study was conducted to explore the multiple roles of biomaterial-based nanocoatings on the cell surface, serving both as a protective shield and an immunomodulator, with a focus on a single disease application.

To circumvent the challenges summarized above, the current study aimed to develop silk-based bioengineered nanoencapsulation strategies to advance immune-regenerative cell therapeutic platforms, thereby attenuating OA conditions. Silk fibroin (hereafter referred to as SF) has been utilized in tissue engineering and regenerative medicine due to its excellent biocompatibility, biodegradability, and unique chemical structure [20]. The unique chemical composition of SF offers a wide range of options for chemical modifications through various SF chemistries, enabling the incorporation of additional functional moieties and biochemical mediators to tailor the material's structure and function further. The exquisite mechanical properties and slow degradation kinetics of SF provided additional advantages of increased retention of the nanocoating on the cell surface. Thus, we exploited the unique versatility of SF biomaterial to generate positively and negatively charged silk ionomers, thereby enhancing the net charge of the protein [21, 22]. With the incorporation of cytokines and functional groups into these silk ionomers, the utility of these new functionalized ionomers in immunomodulation related to OA conditions was systematically investigated. The specific questions addressed included: (i) the effect of LBL coating thickness on barrier functions against different catabolic stresses related to OA; (ii) the immunocompatibility of silk ionomers; (iii) the design of immunomodulatory nanocoatings that preserved chondrocyte viability and phenotype post transplantation to regulate the inflammatory OA niche; (iv) the differentiation of neutral M0 macrophages to M1 and M2 subtypes through the use of cytokine-embedded nanocoatings; (v) further tuning nanoencapsulation stability and retention with spheroids or by introducing tyramine (TA) to the ionomer through chemical modifications. The above goals were investigated through extensive physicochemical and in vitro biological characterization to develop a comprehensive framework that enhances the efficacy of stem cell-based methods, as well as autologous chondrocyte or macrophage-based targeted therapies for OA. The approach also demonstrates opportunities for treating other inflammatory diseases.

2 | Materials and Methods

2.1 | Preparation of Positively Charged and Negatively Charged Ionomer Solutions

Bombyx mori silkworm cocoons were degummed for 60 and 120 min in 0.02 M Sodium Carbonate (Na_2CO_3) (Sigma–Aldrich, St. Louis, MO, USA), respectively and dissolved in 9.3 M Lithium Bromide (LiBr) (Millipore, St. Louis, MO, USA), followed by dialysis in deionized water for 72 h to prepare native silk fibroin (SF) solutions [23]. The cationic ionomer was prepared by reacting native 2% 60 min-boiled SF with Ethylenediamine hydrochloride (EDA) (Millipore, St. Louis, MO, USA) (0.5 g for 1 g of SF) using 1-Ethyl-3-(3-dimethylaminopropyl) carbodiimide (EDC) (Millipore, St. Louis, MO, USA) (84 mg for 1 g of SF) and N-hydroxy succinimide (NHS) (Millipore, St. Louis, MO, USA) (57 mg for 1 g of SF) in 0.05 M (2-(N-morpholino) ethanesulfonic acid saline (MES) buffer (pH *6.0*) at room temperature for 18 h [14, 15]. The anionic ionomer solution was prepared by reacting the diazonium salt solution with the concentrated 10% w/v 120 min-boiled SF solution dissolved in 0.5 M borate buffer (ThermoFisher Scientific, Waltham, MA, USA) at pH *9.0* and incubating it on ice for 20 min. The resulting SF solutions were dialyzed against deionized water using a 3.5 kDa molecular weight cut-off (MWCO) dialysis tube (ThermoFisher Scientific, Waltham, MA, USA) for 5 days, with 10 water changes, to remove excess reactants. The solutions were then centrifuged at 9000 rpm at 4°C for 20 min. The SF solutions were kept in −80°C overnight and lyophilized for further use, with the positively charged SF solution, termed SF-EDA, and the negatively charged SF solution, SF-COOH. The SF-EDA was further labelled with fluorescein isothiocyanate isomer I (FITC) (Millipore, St. Louis, MO, USA) by dissolving it in dimethyl sulfoxide (DMSO), diluting it 4 times and mixing it with 5 mg/mL SF solution in 0.5 M carbonate buffer for 1 h at room temperature (RT) [14]. The resulting solution was dialyzed for 3 days, centrifuged and lyophilized for further use.

2.2 | Procedure of Nanoencapsulation on the Cell Surface

Human mesenchymal stem cells (hMSCs) were isolated from bone marrow aspirates (Lonza Walkersville Inc., Walkersville, MD, USA) under approval from the Institutional Biosafety Committee (IBC) of Tufts University, as described by Li et al. [24]. They were grown in expansion medium comprising Dulbecco's Modified Eagle Medium (DMEM) supplemented with 10% Foetal Bovine Serum (FBS), 1% antibiotic antimycotic, 1% non-essential amino acids, and 10 ng/mL fibroblast growth factor 2 (FGF-2) [25]. The cells at passage 2 were used for nanoencapsulation at a concentration of 1 million cells/mL. To optimize the concentration of the ionomers for nanoencapsulation, the cells were coated with SF solutions at concentrations of 1 and 2 mg/mL for up to 3 bilayers. Each bilayer coating consisted of mixing the cells initially with the SF-EDA solution by gently pipetting, followed by inversion mixing and then centrifuging at 800 g for 1 min at 4°C. The cell pellets were washed with 40 mM HEPES buffer supplemented with 5% w/v dextrose and 50 mM sodium chloride (NaCl) (HD50 buffer). The cell pellets were further suspended in SF-COOH solution by pipette mixing, and the cell pellet post centrifugation was rewashed with HD50 buffer to complete the formation of 1 bilayer. The steps were repeated to form 3-, 6-, and 10-bilayer coatings on the cell surface [14, 15].

2.3 | Evaluating the Stability and Physicochemical Properties of Nanocoating

2.3.1 | Fluorescence Microscopy

To evaluate and optimize the stability of different concentrations and layers on the hMSC surface, FITC-labelled SF-EDA was used as the cationic ionomer, along with an unlabeled anionic ionomer solution (SF-COOH), for encapsulating the cells. The nanocoated cells with different concentrations and bilayers were incubated and imaged at days 1, 3, and 7 using a BZ-X700 fluorescence microscope (Keyence Corp., IL, USA) to assess the persistence of the deposited ionomers.

2.3.2 | Scanning Electron Microscopy (SEM)

The different bilayer nano-encapsulated cells were seeded on 8 μm transwell inserts (Corning Inc., Corning, NY, USA), followed by fixation in 1% glutaraldehyde for 1 h at RT. The cells were then washed with distilled water and subjected to dehydration using a gradient of ethanol concentrations (30%, 50%, 70%, 90%, and 100% w/v). The dehydrated cells were then incubated with hexamethyldisilazane (HMDS; Sigma–Aldrich, St. Louis, MO, USA) to preserve cell morphology and were left in a fume hood overnight for drying. The samples were then sputter-coated with Au-Pd under vacuum and further imaged using an SEM (Zeiss Ultra Plus, Germany) [15].

2.3.3 | Atomic Force Microscopy (AFM)

The hMSCs post-nanocoating were seeded on 8 μm transwell inserts at a density of 10^4 cells/ transwell and imaged using an Asylum Research MFP-3D-Bio AFM (Asylum Research, Santa Barbara, CA, USA) fitted with a NanoWorld Pyrex-Nitride triangular (PNP-TR) AFM probe (Asylum Research, Santa Barbara, CA, USA). The elastic modulus was measured using a 4-point map technique of individual forces vs. indentation curves on 100 μm^2 of the hMSC cell surface [15, 17].

2.4 | Evaluating the Cytocompatibility and Immunocompatibility of the Nanocoatings

2.4.1 | Cytocompatibility

The hMSCs post-encapsulation with different SF concentrations and bilayers were evaluated for cell viability using a Live Dead assay kit (Invitrogen, Carlsbad, CA, USA) following the manufacturer's protocol. Briefly, the cells were incubated on different days, 1, 3, and 7, with a 2 μM Calcein and 4 μM Ethidium Homodimer (EthD-1) solution for 30 min in the dark, followed by imaging using a BX700 Fluorescence Microscope (Keyence Corp., IL, USA) [26]. Alamar blue assay was carried out to evaluate the cell proliferation index of the hMSCs at different time intervals post-encapsulation. The encapsulated cells were incubated with 10% w/v alamar blue solution (Invitrogen, Carlsbad, CA, USA) for 3 h, and the fluorescence intensity was measured at 630 nm using a UV–vis spectrophotometer (ThermoFisher Scientific, Waltham, MA, USA). The metabolic activity of the nano-encapsulated cells on day 7 was evaluated using the 3-(4,5-dimethylthiazol-2-yl)-2,5-diphenyltetrazolium bromide (MTT) assay kit (Abcam), following the supplier's protocol. Briefly, 50 μL of media and 50 μL of MTT solution were added to each well in a 1:1 ratio, and the mixture was incubated at 37°C for 3 h. Following this, 150 μL of MTT solvent was added to the respective wells, and the mixture was shaken in an orbital shaker for 15 min. The absorbance was recorded at 590 nm using a UV–vis spectrophotometer (ThermoFisher Scientific, Waltham, MA, USA).

2.4.2 | Immunocompatibility

The immunocompatibility of the nanocoatings was evaluated by using two different cell types: THP-1 Apoptosis-associated speck-like protein containing Caspase recruitment domain (THP-1 ASC) and Human Embryonic Kidney 293 cells engineered to express Interleukin 1 beta (HEK-IL-1β) reporter cell lines. Briefly, THP-1 ASC reporter cells (Invivogen, San Diego, CA, USA) were cultured in Roswell Park Memorial Institute Medium (RPMI, Gibco, Waltham, MA, USA) supplemented with 10% FBS (Gibco, Waltham, MA, USA) and 1% antibiotic-antimycotic (Gibco, Waltham, MA, USA) [27]. The cells at passage 4 were seeded in a 48-well plate at a density of 150 000 cells/mL with phorbol myristate acetate (PMA) (Sigma–Aldrich, St. Louis, MO, USA) overnight to convert them into adherent M0 macrophages. The M0 macrophages were then treated with 12 mg/mL SF-EDA, SF-COOH, and SF, and 1 μg/mL Lipopolysaccharide (LPS, Sigma–Aldrich, St. Louis, MO, USA), respectively. They were observed under a fluorescence microscope for green speck formation at 24 and 72 h. The media samples from the macrophage culture, post-treatment with different SF solutions, were collected at 24 and 72 h,

respectively, and used to culture the HEK-IL-1β reporter cell lines according to the manufacturer's protocol. HEK- IL-1β reporter cell lines (Invivogen, San Diego, CA, USA) were expanded in complete medium comprising DMEM supplemented with 10% FBS and 1% antibiotic-antimycotic. The cells at 80% confluency were seeded overnight in a 96-well plate with 50 µL of THP-1 ASC media (collected at different time points) and 150 µL of HEK-IL-1β media. The release of cleaved IL-1β was evaluated using the QUANTI-blue assay (Invivogen, San Diego, CA, USA) as a function of released secreted embryonic alkaline phosphatase (SEAP) by the HEK-IL-1β reporter cell lines, and absorbance was measured at 630 nm using a UV-spectrophotometer (ThermoFisher Scientific, Waltham, MA, USA).

2.5 | Differentiation Potential of the hMSCs After Nano-Encapsulation

The hMSCs, post-encapsulation with two different concentrations of SF solutions (1 and 2 mg/mL) in 3 bilayers, were seeded in a 48-well plate at a density of 20 000 cells/mL in expansion medium for 72 h, followed by chondrogenic differentiation medium for the next 14 days. The chondrogenic differentiation medium was comprised of DMEM/F12 (Gibco, Waltham, MA, USA) supplemented with 1% antibiotic-antimycotic (Gibco, Waltham, MA, USA), 1% sodium pyruvate (Gibco, Waltham, MA, USA), 1% HEPES buffer (Gibco, Waltham, MA, USA), 1% insulin-transferrin-selenium (ITS) + premix (Gibco, Waltham, MA, USA), 10 ng/mL transforming growth factor beta 3 (TGFβ3; Peprotech, NJ, USA), 10^{-7} M dexamethasone (Sigma Aldrich, St. Louis, MO, USA), and 0.1 mM ascorbic acid 2-phosphate (Sigma–Aldrich, St. Louis, MO, USA) [28]. Post 14 days of differentiation, the cells were fixed with 4% paraformaldehyde (ThermoFisher Scientific, Waltham, MA, USA), permeabilized with 0.1% Triton-X100 (Invitrogen, Carlsbad, CA, USA), blocked using 2% bovine serum albumin (BSA; Invitrogen, Carlsbad, CA, USA) and then stained with chondrogenic marker collagen type-II primary (COL-II) (Rabbit; 1:200 dilution; Abcam), aggrecan (ACAN) (Mouse; 1:200 dilution; Abcam), collagen type-X (COL-X) (Mouse; 1:200 dilution; Abcam) overnight at 4°C. The samples were further stained with secondary antibodies, Alexa Fluor 488 (anti-mouse; 1:250 dilution; Invitrogen, Carlsbad, CA, USA) and Alexa Fluor 546 (anti-rabbit; 1:250 dilution; Invitrogen, Carlsbad, CA, USA), respectively, followed by nucleus stain 4',6-diamidino-2-phenylindole (DAPI; 1:500 dilution; Invitrogen, Carlsbad, CA, USA) and imaged using a BX-700 fluorescence microscope (Keyence Corp., IL, USA). A similar procedure was repeated for 3-bilayer and 6-bilayer nano-encapsulated cells using an optimized SF concentration of 2 mg/mL.

2.6 | Evaluating the Fate of the Nanocoatings in the Body

The 6 bilayer-coated hMSCs, with 2 mg/mL FITC-labelled SF-EDA and SF-COOH, were seeded in a 48-well plate at a density of 100 000 cells/mL and cultured for 72 h. Parallelly, THP-1 monocytes at a density of 100 000 cells/mL were converted to M0 macrophages using 150 nM PMA overnight. The media from the 72 h culture of nano-encapsulated cells were then used to culture the macrophages for 24 h. The potential of macrophages to phagocytose the nanocoating fragments in the media was investigated at 4 and 24 h, respectively, using flow cytometry.

2.7 | Evaluating the Protective Nature of the Nanocoatings

2.7.1 | Simulated Joint Microenvironmental Stress Conditions

The cells after encapsulation with 1 and 2 mg/mL of SF-EDA and SF-COOH solutions and non-coated controls were seeded in a 96 healthy plate at a cell density of 10 000 cells/well in expansion medium for 24 h and then changed to different joint microenvironment stressor mediums for the next 72 h: (a) **Inflammation**: 0.05 ng/mL of Interleukin 1 beta (IL-1β, Peprotech, NJ, USA), 0.05 ng/mL of Tumor Necrosis Factor alpha (TNFα, Peprotech, NJ, USA) and 0.1 ng/mL of Interleukin 6 (IL-6, Peprotech, NJ, USA) [29]; (b) **Oxidative stress**: 0.1 and 0.5 mM of hydrogen peroxide [30] (H_2O_2; Sigma–Aldrich, St. Louis, MO, USA) (c) **Protease Stress**: 0.01 and 0.05 U of Protease XIV [31] (Sigma–Aldrich, St. Louis, MO, USA); (d) **Hypoxia stress**: 0.1 and 0.5 mM of Cobalt Chloride [32] ($CoCl_2$, Sigma–Aldrich, St. Louis, MO, USA); and (e) **Cocktail**: Combination of 0.05 ng/mL of IL-1β, 0.05 ng/mL of TNFα and 0.1 ng/mL of IL-6, 0.5 mM of H_2O_2, 0.05 U of Protease XIV and 0.5 mM of $CoCl_2$. After 72 h of post-treatment, the cells were stained with a Live/Dead assay kit (Invitrogen, Carlsbad, CA, USA) to assess cell viability, and cell proliferation was estimated using the Alamar Blue assay (Invitrogen, Carlsbad, CA, USA). Any inclination toward apoptosis post-incubation in the stressor medium was analyzed using the Lactate Dehydrogenase (LDH) assay (Sigma–Aldrich, St. Louis, MO, USA) according to the supplier's instructions. Briefly, the LDH assay mixture was prepared by mixing equal volumes of LDH dye solution, LDH substrate solution, and the cofactor. The freshly prepared LDH assay mixture and media samples collected from the treated cells were mixed in a 2:1 ratio in a 96-well plate and incubated in the dark for 30 min. The absorbance was recorded at 490 nm using a UV spectrophotometer (ThermoFisher Scientific, Waltham, MA, USA).

2.7.2 | Simulated Joint Mechanical Stress

The 3- and 6-bilayer nano-encapsulated hMSCs, with optimized 2 mg/mL SF-EDA and SF-COOH ionomers, respectively, along with a non-coated control, were subjected to mechanical stress using a plate and plate ARES-LS2 rheometer (TA Instruments) [12]. The cells were placed on the bottom plate, and an 8 mm top plate was used to exert shear force on the cells at a constant shear strain of 1000% and shear stress of 1 MPa for 150, 300, and 600 s, respectively, to mimic the joint mechanical stressor condition. Following exposure to stress, the cells were assessed for cell viability and inclination toward apoptosis using Live/Dead staining, Alamar Blue, and LDH assays, respectively, as described in Section 2.7.1.

2.7.3 | Syringe Extrusion

The hMSCs with 3 and 6 bilayer nanocoatings along with non-coated control were loaded in a 1 mL syringe (BD Biosciences) at a cell density of 1 million cells/mL and extruded with a 32-gauze needle (inner diameter: 76 μm) using a Harvard PHD 2000 syringe pump (Harvard Apparatus, Holliston, MA, USA) at a volumetric flow rate of 150 μL/minute. After extrusion, the cells were stained with EthD-1 (Invitrogen, Carlsbad, CA, USA) to identify dead cells, followed by imaging under a BX-700 fluorescence microscope (Keyence Corp., IL, USA). The extruded cells were incubated for 2 h post-extrusion and then quantified for cell survival using an Alamar blue (Invitrogen, Carlsbad, CA, USA) assay.

2.8 | Developing a Cytokine-Immobilized Nanocoating for Immunomodulation

2.8.1 | Anti-Inflammatory Coated Human Chondrocytes Promote Re-Polarization of Pro-Inflammatory M1 Macrophages to a Healing M2 Phenotype

The human chondrocytes (ScienceCell, Carlsbad, CA, USA) were expanded in DMEM high glucose + Glutamax (Gibco, Waltham, MA, USA) supplemented with 10% FBS, 1% antibiotic antimycotic, 1% HEPES buffer and 1% sodium pyruvate. The cells at passage 2 were used for nanoencapsulation. Briefly, cells at a density of 1 million/mL were initially encapsulated with 2 mg/mL SF-EDA and SF-COOH solutions for 6 bilayers and evaluated for stability (FITC labeling and fluorescence microscopy) and cytocompatibility (Live/Dead and Alamar Blue) over 7 days (as described in sections 2.3.1 and 2.4.1 respectively).

The THP-1 monocytes were seeded at a density of 150 000 cells/mL into each 48-well plate and converted to adherent M0 macrophages using 150 nM PMA [33]. The M0 macrophages were then polarized into pro-inflammatory M1 macrophages by supplementing the media with 50 ng/mL Interferon gamma (IFNγ) + 100 ng/mL LPS for 72 h. The conversion of M0 to M1 was validated by staining with pro-inflammatory M1 marker CD86. The chondrocytes were encapsulated with 2 mg/mL of 3- and 6-bilayer anti-inflammatory coatings comprising SF-EDA and SF-COOH, immobilized with 500 ng/mL IL-1Ra, 50 ng/mL IL-4, and 50 ng/mL IL-13. The anti-inflammatory coated chondrocytes were incubated in hypertrophic differentiation medium for 7 days [25] and evaluated for the onset of chondrocyte hypertrophy by immunostaining of chondrocyte hypertrophy markers, COL-X and runt-related transcription factor 2 (RUNX2), similarly as described in Section 2.5. The chondrocytes post-encapsulation was co-cultured with the pro-inflammatory M1 macrophages and incubated for 72 h, allowing the M1 macrophages to re-polarize to M2. The M2 repolarization was confirmed by co-staining the cells with M1-specific marker CD86 and M2-specific marker CD206 and calculating the M1/M2 ratio using ImageJ software.

2.8.2 | Coating-Directed Polarization of M0 Macrophages Polarization

The SF-EDA and SF-COOH cationic and anionic ionomer solutions were immobilized with pro- and anti-inflammatory cytokines to ensure in situ macrophage polarization from the localized delivery of the cytokines to the cells. A combination of cytokines has been initially optimized to induce the optimal conversion of macrophage phenotypes from the neutral M0 phenotype, balancing both anti-inflammatory and pro-inflammatory effects. The technical details of the cytokines have been enlisted in Figure S1. The THP-1 monocytes (ATCC, Manassas, VA, USA) were initially expanded in RPMI medium (Gibco, Waltham, MA, USA) supplemented with 10% FBS and 1% antibiotic-antimycotic and then polarized to adherent M0 macrophages by supplementing the expansion medium with 150 nM PMA overnight. The M0 macrophages were then conditioned with anti-inflammatory cytokine cocktails (500 ng/mL Interleukin 1 receptor antagonist (IL-1Ra, Peprotech, NJ, USA) + 50 ng/mL IL-4 (Peprotech, NJ, USA) + 50 ng/mL IL-13 (Peprotech, NJ, USA)) for 72 h for M2 polarization. The M0 macrophages were also conditioned with a pro-inflammatory cytokine cocktail (50 ng/mL of IFNγ (Peprotech, NJ, USA) + 100 ng/mL LPS (Sigma Aldrich, St. Louis, MO, USA)) for 72 h for M1 polarization. After 72 h incubation, the cells were fixed with 4% paraformaldehyde, permeabilized with 0.1% Triton X-100, and blocked with 2% BSA. The cells were then stained with CD206 (Rabbit; 1:200 dilution; Abcam) and CD86 (Mouse; 1:200 dilution; Abcam) primary antibodies, followed by Anti-rabbit Alexa 546 (1:250 dilution; Invitrogen, Carlsbad, CA, USA) and anti-mouse Alexa Fluor 488 (1:250 dilution; Invitrogen, Carlsbad, CA, USA) secondary antibodies and DAPI (1:500 dilution; Invitrogen, Carlsbad, CA, USA), and imaged in a BX-700 fluorescence microscope (Keyence Corp. IL, USA). Once polarization was confirmed, the optimized concentration and combination of anti-inflammatory and pro-inflammatory cytokines were immobilized into each SF-EDA and SF-COOH ionomer solution before nano-encapsulation. The neutral M0 macrophages were then trypsinized and encapsulated with anti-inflammatory and pro-inflammatory coatings at a density of 1 million cells/mL, and incubated for 72 h. The polarization of the neutral M0 macrophages to pro-inflammatory M1 and anti-inflammatory M2 has been confirmed through immunostaining with respective M2-specific (CD206 (Rabbit; Abcam; 1:200 dilution) and Arginase (Rabbit; Abcam; 1:200 dilution) and M1-specific markers CD86 (Mouse; Abcam; 1:200 dilution) and iNOS (Mouse; Abcam; 1:200 dilution). From here, 'anti-inflammatory coating' refers to the anti-inflammatory cytokine-embedded ionomers, 'inflammatory coating' refers to the pro-inflammatory cytokine immobilized ionomers and 'standard coating' refers to the general SF-EDA and SF-COOH ionomers.

2.8.3 | Coating-Directed Polarization of Macrophages and THP-1 ASCs

The THP-1 ASCs were expanded as described in Section 2.4.2. The cells, at a density of 1 million/mL, were encapsulated with the pro-inflammatory nanocoating (as described in Section 2.8.1) and incubated for 72 h. The cells were imaged for green fluorescence speck formation at 24 and 72 h, respectively, using a BX-700 fluorescence microscope (Keyence Corp., IL, USA). The secreted cleaved IL-1β was quantified using media samples collected at 24 and 72 h, and HEK-IL-1β reporter cell lines were used following the QUANTI-Blue assay (described in Section 2.4.2).

2.8.4 | Immunomodulatory Effect of the Anti-Inflammatory Coated M0 Macrophages on the Inflammatory Synovial Fibroblasts

Human synovium from healthy donors was obtained from the Musculoskeletal Transplant Foundation (MTF, Edison, NJ, USA), where the tissue collection was deemed exempt from IRB review. The explants were trimmed of excess adipose and outer capsule tissue before digestion and cell isolation. The explants were then digested in collagenase solution for 5 h, filtered and plated. The cells were expanded in Minimum Essential Medium- alpha modification (α-MEM) supplemented with 10% FBS, 1% antibiotic antimycotic and 5 ng/mL FGF-2 [34]. The cells at passage 2 were seeded at a density of 50,000 cells/mL in a 48-well plate and incubated with 0.01 μg/mL IL-1β for 72 h to induce inflammation. The anti-inflammatory coated M0 macrophages (IL-4 + IL-13 + IL-1Ra) were directly seeded on the inflammatory synovial fibroblasts and incubated for another 72 h. The synovial fibroblasts were stained for arthritic synoviocyte marker α-smooth muscle actin (α-SMA; Abcam; 1:200 dilution), and the media samples were collected for quantifying the cleaved IL-1β secretion by initially culturing with HEK-IL-1β reporter cell lines, followed by QUANTI-Blue assay by measuring the secreted embryonic alkaline phosphatase (described in Section 2.4.2).

2.9 | Effect of Nanocoatings on 3D Cell Aggregates

Human MSCs were expanded till passage 2 (as described in Section 2.2) for spheroid formation. Briefly, the cells were trypsinized at 80% confluency and counted for seeding into an ultra-low adherence 96 U-bottom plate (Nunclon, ThermoFisher Scientific, Waltham, MA, USA) at a cell density of 10 000 and 20 000 cells/mL [9]. The cells were allowed to grow for 72 h and observed under a bright-field microscope (EVOS) for the formation of rigid spheroids.

2.9.1 | Nanoencapsulation of Spheroids

The 10 000 and 20 000 cell/mL spheroids were encapsulated with 2 mg/mL 6 bilayer SF-EDA (FITC-labelled) and SF-COOH ionomers following a similar protocol mentioned in Section 2.2 with minor modifications. Briefly, the media from the wells were removed, and the spheroids were washed with HD50 buffer for 2 min. The spheroids were then incubated in FITC-labelled SF-EDA ionomer solution for 2 min in an orbital shaker and washed with HD50 buffer. The orbital shaker allows for homogeneous coating deposition on the spheroid's surface. The spheroids were then incubated with the SF-COOH solution in an orbital shaker and washed again with HD50 buffer to complete 1 bilayer. The previous steps were repeated 5 times to deposit a 6-bilayer coating on the spheroid surface.

2.9.2 | Evaluating the Coating Stability and Viability of the Spheroids Post-Encapsulation

For assessing the stability of the nanocoatings, the FITC-labelled ionomer-coated spheroids were stained with phalloidin (1:400 dilution; Invitrogen, Carlsbad, CA, USA) and DAPI (1:500 dilution; Invitrogen, Carlsbad, CA, USA) and imaged using a TCS SP8 Confocal microscope (Leica Microsystems, Wetzlar, Germany) at days 1 and 7, respectively, for both 10 000 and 20 000 cells/mL spheroids. Representative fluorescence images were captured using an Asylum Research MFP-3D-Bio AFM microscope to show the deposition of the ionomers. To compare the stability of the nanocoatings on single cells vs. spheroids, the FITC-labelled SF-EDA and SF-COOH coated spheroids and single cells were seeded at the same cell density in a 96 flat-bottom (Nunc) and 96 U-bottom plates (Nunclon, ThermoFisher Scientific, Waltham, MA, USA), respectively. The media samples at days 1, 3, and 7 were collected from both the experimental groups and the fluorescence intensity was recorded using a UV spectrophotometer (ThermoFisher Scientific, Waltham, MA, USA) (λ_{ab}: 495 nm; λ_{em}: 519 nm). The hypothesis lies in the lower fluorescence intensity values corresponding to a reduced quantity of FITC in the media samples, hence, a more stable coating on the spheroid surface. The viability of the spheroids after encapsulation was evaluated using the Alamar Blue assay.

2.9.3 | Evaluating the Protective Nature of the Nanocoatings From Microenvironmental Stress and Inflammatory Immune Cell Attack

The 6-bilayer nanocoated spheroids were incubated in a cocktail stress medium for 72 h, and the protective nature of the nanocoating was evaluated using Alamar Blue and LDH assays as described in Section 2.7.1. The infiltration of the pro-inflammatory immune cells into the 3D cell aggregate was initially achieved by labelling the macrophages with a fluorescent red dye. Briefly, the THP-1 monocytes were converted to M0 macrophages with 150 nM PMA, followed by polarization into pro-inflammatory M1 macrophages using 50 ng/mL IFNγ and 100 ng/mL LPS for 72 h. The M1 macrophages were then trypsinized and labeled with Vybrant Multicolor Cell-Labeling Kit (Invitrogen, Carlsbad, CA, USA) according to the manufacturer's protocol. Briefly, 5 μL of dye solution was added per 1 million cells, followed by incubation at 37°C for 30 min. The cells were then washed twice with THP-1 expansion medium. The labelled M1 macrophages were then added to the 6-bilayer nano-encapsulated spheroids at a density of 20 000 cells/mL and incubated for 7 days. The macrophage-nanocoated spheroid co-culture system was imaged at different time points using a laser scanning TCS SP8 confocal microscope (Leica Microsystems, Wetzlar, Germany).

2.10 | Developing a Tunable Tyramine-Substituted Ionomer (SF-EDA-TA) for Enhanced Stability

2.10.1 | Ionomer Synthesis

The tyramine-substituted SF-EDA ionomer solution (SF-EDA-TA) was synthesized as described in Section 2.1 with minor modifications. The cationic ionomer was prepared by reacting native 2% 60 min-boiled SF solution with EDA (0.25 g for 1 g of SF) and tyramine hydrochloride (TA) (0.25 g for 1 g of SF) in 1:1 ratio using EDC (84 mg for 1 g of SF) and NHS (57 mg for 1 g of SF) in 0.05 M MES buffer (pH *6.0*) at RT for 18 h. The solution was then

dialyzed in DI water for 5 days in a dialysis tube (MWCO: 3.5 kDa) with 10 water changes. The final solution was centrifuged twice at 9000 rpm for 20 min to remove aggregates, frozen at −80°C, lyophilized, and the powders were stored at −20°C until further use.

2.10.2 | Characterization of the SF-EDA-TA Ionomer

The Fourier Transform Infra-red spectroscopy (FTIR) was performed using a JASCO FTIR 6200 spectrometer (JASCO, Tokyo, Japan) to determine and compare the secondary structure conformations in SF-EDA and SF-EDA-TA ionomers. A total of 64 scans were carried out with a resolution of 4 cm^{-1} per scan, spanning the range from 400 to 4000 cm^{-1}. The percentage beta sheet content was calculated using the Fourier self-deconvolution method (Lorentz deconvolution) between 1616 and 1637 cm^{-1} using Origin 2020 (OriginLab, Northampton, MA). ^{1}H NMR was also performed to confirm the chemical modification of SF-EDA with the tyramine substitution. The lyophilized samples were reconstituted in deuterated water (D2O), transferred to a ^{1}H NMR tube, and measured using a 500 MHz Bruker NMR spectrometer. The data analysis was carried out using Top Spin 3.6.1 software. For zeta potential measurement, the SF-EDA and SF-EDA-TA lyophilized samples were reconstituted in distilled water at a concentration of 5 mg/mL and measured using NanoBrook ZetaPALS (Brookhaven Instruments, Holtsville, NY, USA). The corresponding zeta potential values were calculated using the Smoluchowski model [14]. Sodium dodecyl sulfate Polyacrylamide gel electrophoresis (SDS-PAGE) was used to estimate the change in the molecular weight of SF-EDA post-substitution with TA. Briefly, 1% SF-EDA-TA and SF-EDA solutions were mixed with LDS buffer (Invitrogen, Invitrogen, Carlsbad, CA, USA; NuPAGE) and a reducing agent, and then heated at 70°C for 10 min before being loaded into the wells, along with the reference ladder (Invitrogen, Carlsbad, CA, USA; Pre-Stained Protein Standard). The gel was run in 1X MES buffer at 200 V for 30 min and stained as previously described [35]. Briefly, the gels were incubated in fixing solution for 10 min, followed by staining solution A for an additional 10 min and staining solution B for 3 h. The gel was rinsed with ultrapure distilled water before being washed overnight and imaged. The gel was imaged in a gel imager, and the corresponding molecular weight was calculated using ImageJ software [35]. The water contact angle (WCA) was measured by drop-casting 5% w/v SF-EDA and SF-EDA-TA biopolymer solutions on a glass slide and allowing for overnight drying before water annealing the films for 4 h at a constant vacuum (−25 inHg or −85 kPa) to achieve water stability. The corresponding contact angle was measured using a goniometer with a 10 µL water drop [36].

2.10.3 | Stability and Cytocompatibility of the SF-EDA-TA Nanocoatings on Stem Cells and Immune Cells

The SF-EDA-TA solution was previously labeled with Rhodamine-B-isothiocyanate (RBITC) using a protocol similar to that for FITC labeling (Section 1.2). The hMSCs and THP-1 cells were encapsulated with 2 mg/mL of RBITC-labelled SF-EDA-TA and SF-COOH up to 6 bilayers at a density of 1 million cells/mL. The encapsulation was carried out using two protocols: a) crosslinked and b) non-crosslinked. The introduction of crosslinking using the horseradish peroxidase (HRP) enzyme and H_2O_2 into the tyramine-substituted SF-EDA was hypothesized to enhance the stability of the coating by forming di-tyrosine bonds [37]. For the crosslinked coating protocol, the SF-EDA-TA ionomer solution was mixed with 10 U/mL HRP and 0.001% H_2O_2 and incubated at 37°C for 2 h before nano-encapsulation. The persistence of the nanocoating on the cell surface was assessed by imaging under the BZ-X700 fluorescence microscope (Keyence Corp., IL, USA) at days 1, 3, and 7. The viability of hMSCs and THP-1 cells post-coating with SF-EDA-TA was evaluated using corresponding live/dead staining and Alamar Blue assays, respectively, on days 1, 3, and 7.

2.10.4 | Stability of the SF-EDA-TA Coating in 3D Aggregates

The hMSCs were coated using 2 mg/mL crosslinked RBITC-labelled SF-EDA-TA for 6 bilayers. The coated cells were then seeded at a density of 20 000 cells/mL in an ultra-low attachment 96-well U-bottom plate (Nunclon, ThermoFisher Scientific, Waltham, MA, USA) to form spheroids. The spheroids were then imaged using a laser scanning TCS SP8 confocal microscope (Leica Microsystems, Wetzlar, Germany) at days 1, 3, and 7 to assess the stability of the coatings on the cell surface, and the corresponding fluorescence intensity was calculated using ImageJ.

2.11 | Statistical Analysis

One-way analysis of variance (ANOVA) with Tukey's *post-hoc* multiple comparison tests was carried out to compare among more than two experimental groups, whereas an independent non-parametric *t*-test was employed when comparing between two groups using GraphPad Prism 8 (GraphPad Software) to estimate the statistical significance *($*p < 0.05$, $**p < 0.01$ and $***p < 0.001$)*. All experiments were conducted in independent sample replicates ($n \geq 3$), and the quantitative data are presented as mean ± standard deviation. The % cytocompatibility (Alamar blue) and MTT assay results have been normalized to non-coated control to evaluate the effect of nanocoating on cell proliferation and metabolic activity. All the % cell viability (Alamar blue assay) results have been normalized to non-coated control and 3-bilayer and 6-bilayer nanocoated controls without exposure to microenvironment and biomechanical stressors to quantify the protective function. GraphPad Prism 8 software has been used for graph plotting whereas ImageJ software has been used for image processing and quantification.

3 | Results and Discussion

3.1 | Silk Ionomer Nanocoatings did not Alter hMSCs' Functions

The SF-EDA and SF-COOH ionomer-based nanocoatings provided an additional layer of temporary protection to the hMSCs by creating an artificial cell wall (Figure 1a,b). The 2 mg/mL demonstrated enhanced stability as a cell coating compared to

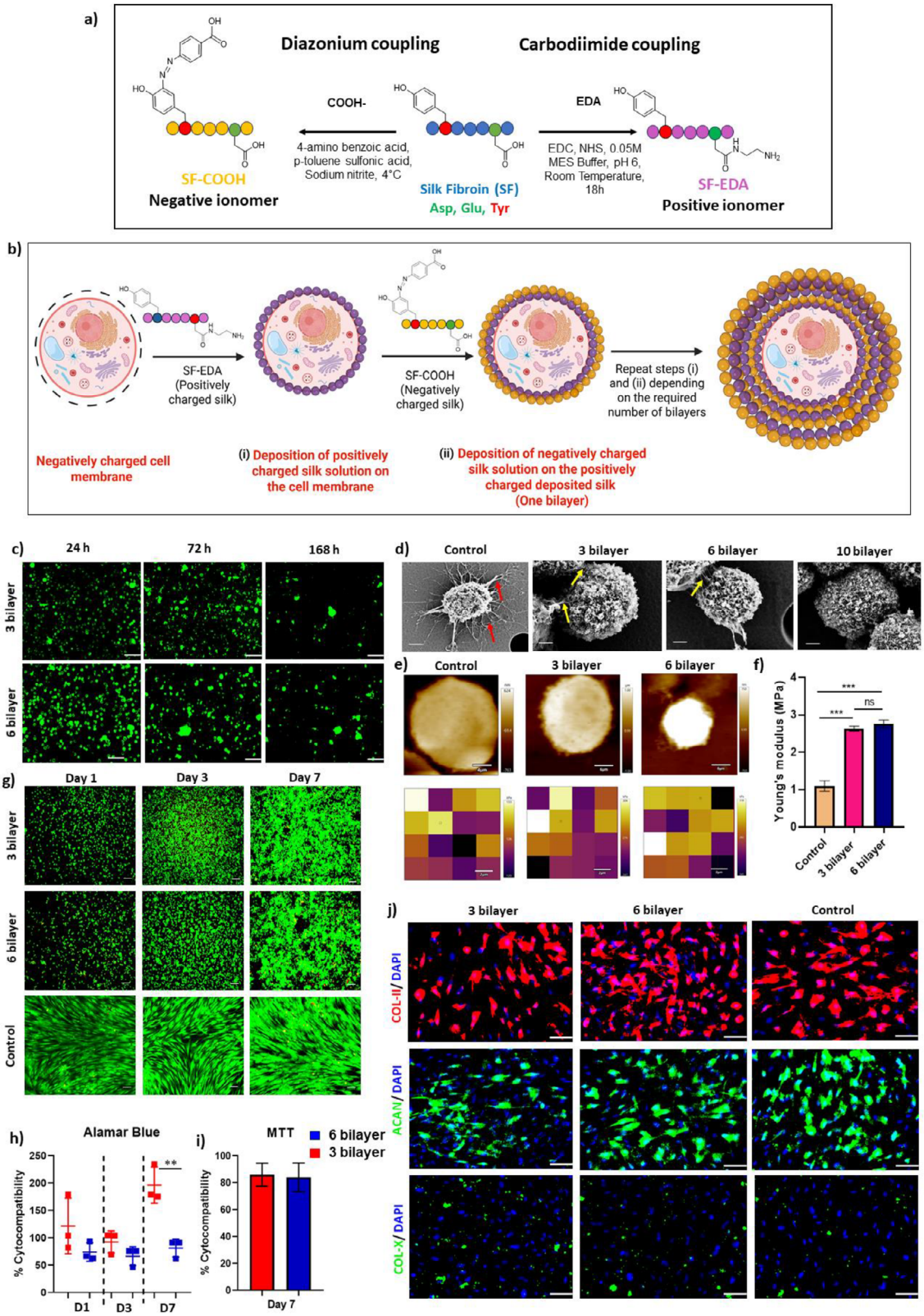

FIGURE 1 | The layer-by-layer deposition of silk ionomer nanocoating preserved the viability, proliferation, metabolic activity and differentiation potential of hMSCs. (a) Chemical synthesis of the cationic and anionic silk ionomers through carbodiimide and diazonium chemistries, (b) Nanoencapsulation mechanism of LBL deposition of the cationic and anionic silk ionomers on the cell surface, (c) Fluorescence microscopy images demonstrating the stability of the nanocoatings on the cell surface up to 72 h with further aggregation at 168 h (day 7) (Scale bar: 100 μm), (d) SEM micrographs illustrating the successful deposition of nanocoating on the cell surface (Scale bar: 2 μm), (e) Topographic image of non-coated control (Scale bar: 4 μm), 3-bilayer and 6-bilayer (Scale bar: 6 μm) nanocoated MSCs using contact mode of AFM, (f) Bar graph comparing the Young's modulus of the 3-bilayer and 6-bilayer nanocoated hMSCs with the non-coated control until day 7*(*$p < 0.05$, **$p < 0.01$ and ***$p < 0.001$)*, (g) Live/dead imaging

1 mg/mL for up to 72 h, with the formation of fewer cell aggregates and slower detachment from the cell surface (Figure S2). Furthermore, the 1 and 2 mg/mL bilayer coatings did not affect the overall cell viability, proliferation (Figure S3), or differentiation (Figure S4) of the hMSCs post-encapsulation, while protecting the cells from various environmental stresses (Figure S5). Thus, 2 mg/mL of silk ionomer was chosen to encapsulate the cells with 3 and 6 bilayers, respectively, for all further downstream experiments. The fluorescence microscopy images revealed that the coatings persisted on the cell surfaces for 72 h (Figure 1c), with the 3-bilayer coating disengaging faster than the 6-bilayer coating. The faster detachment of the 3-bilayer nanocoating compared to the 6-bilayer coating at 168 h can be primarily attributed to weaker electrostatic interactions resulting in a less compact, mechanically fragile network prone to premature disengagement. Additional factors, like hydration dynamics [38], protein corona formation on the silk surface, [39–41] or matrix metalloproteases (MMP-1/13) secreted by hMSCs [42], can accelerate the nanocoating degradation on the cell surface. SEM micrographs demonstrated a flaky deposition of random coil-like silk fibres covering the cell surface with no visible cellular projections in the 3,6, and 10 bilayer-coated hMSCs (Figure 1d (red arrows)). This is in line with the nanocoating studies on neural stem cells and L929 fibroblast cell surfaces [14, 43]. In contrast, strong adherence and cellular extensions have been observed in the non-coated controls. The approximate dimensions of the cells were measured from the SEM micrographs, indicated a decrease in size with an increase in bilayer deposition from 156.89 ± 13.06 μm in the non-coated control, 134.88 ± 23.42 μm for 3-bilayer, 125.36 ± 15.91 μm for 6-bilayer and 113.13 ± 31.76 μm for 10-bilayer samples (Figure S6). However, there is no statistical significance between the different non-coated and nanocoated groups. The SEM micrographs of the encapsulated cells morphologically showed the formation of cellular bridges (Figure 1d (yellow arrows), with neighbouring cells exhibiting no inhibition of cell-to-cell connections [44, 45]. AFM nanoindentation measurements showed a significant increase in elastic modulus between the coated and the non-coated cells, with no significant difference in elastic modulus between 3 (263.92 ± 6.1 kPa) and 6 bilayers (275.97 ± 9.23 kPa) (Figure 1e,f). Therefore, it can be inferred that encapsulating the cells with the SF-EDA and SF-COOH ionomers increased the overall stiffness of the cells. However, increasing the number of bilayers above 3 had no significant effect on stiffness, a similar observation to that for nanocoated THP-1 cells [15]. The plateau could be attributed to the stabilization of the coating, with no increase in layer thickness, and structural loosening due to poor electrostatic interaction caused by charge stabilization after 5 bilayers. Such an elastic modulus of the surrounding nanocoating is suitable for chondrogenic differentiation of the stem cells. While an increase in the number of coating bilayers would intuitively suggest a larger apparent cell dimension, the reduction in surface height observed in the 6-bilayer group likely reflects interpenetration and densification of adjacent SF-ionomer layers during sequential deposition. The repeated layering process promotes enhanced β-sheet formation, which increases coating stiffness and structural order through extensive hydrogen bonding [46]. This transition from a more hydrated, amorphous structure (3-bilayer) to a compact, crystalline network (6-bilayer) result in a mechanically rigid, thinner shell. Such densification can also mechanically constrain the plasma membrane, limiting osmotic expansion and inducing mild cytoskeletal compaction [47, 48]. Together, these effects account for the smaller apparent cell dimension with the 6-bilayer coating in the AFM topography. Following conformation of nanocoating deposition and stability, the immediate step would be to observe how the nanocoating on the cell surface influences the cytocompatibility with the hMSCs.

A preliminary finding for the SF-based nanocoating system was its non-interference with the viability, proliferation and metabolic activity of the stem cells. The live-dead micrographs showed a negligible effect of nanoencapsulation on the viability of hMSCs, displaying a spherical morphology compared to the non-coated cells with a spindle appearance (Figure 1g). [48, 49] The 6-bilayer coating resulted in a reduction in cytocompatibility (measured as a function of cell proliferation using Alamar blue) (66.32% ± 17.14%) compared to the 3-bilayer (92.62% ± 19.98%) until day 3 of culture, beyond which the proliferation rate increased significantly (Figure 1h). However, the metabolic activity of the nano-encapsulated hMSCs was not compromised for 3 (85.97% ± 6%) and 6-bilayers (84% ± 7.49%) at day 7 (Figure 1i). Hence, the 6-bilayer encapsulation caused a decrease in the proliferation capacity of the hMSCs but maintained the metabolic activity of the cells, a characteristic feature of G_0 or quiescent cells [49]. Our data indicate that during the 72-h persistence of the nanocoating, cell proliferation is transiently suppressed but fully recovers once the coating begins to disengage (Figure 1h). This transient quiescence likely reflects a mechanically induced growth-arrest state rather than canonical G_0 entry. The SF-ionomer coating forms a conformal, non-adherent shell that restricts integrin engagement and cytoskeletal tension, both of which are essential for cell cycle progression. [50] as illustrated in Figure S7. Such loss of adhesion signaling has been reported to downregulate cyclins and sustain cells in a G_0-like, metabolically active but non-dividing condition until mechanical constraints are released [51]. Once the coating sheds after ~72 h, restored matrix contact reactivates proliferation, consistent with our observed recovery by day 7. Additionally, some cellular aggregation has been observed for the 6-bilayer nanocoated hMSC group from day 3, which further increased at day 7, significantly reducing the proliferation potential of the cells due to contact inhibition and necrotic core formation.

However, a 14-day chondrogenic differentiation induction study was conducted next to evaluate whether the early coating phase (~72 h), during which cell-matrix interaction is inhibited, impacts the chondrogenic differentiation of hMSCs. The 3- and 6-bilayer coated hMSCs, when incubated with chondrogenic differentiation medium for 14 days post-encapsulation, demonstrated suc-

showing the viability of the hMSCs post nano-coating (Scale bar: 100 μm), (h) Quantification of cell proliferation after nanoencapsulation at days 1, 3 and 7 using Alamar blue assay (*$p < 0.05$, **$p < 0.01$ and ***$p < 0.001$)(normalized to the non-coated control Alamar blue data), (i) Quantification of metabolic activity of the hMSCs post 3 and 6-bilayer nanocoating at day 7 (*$p < 0.05$, **$p < 0.01$ and ***$p < 0.001$))(normalized to the non-coated control Alamar blue data), and (j) Intact differentiation potential of the hMSCs post-nanocoating (Scale bar:100 μm).

cessful chondrogenic differentiation. This is supported marked expression of hyaline cartilage marker COL-II and ACAN and downregulated expression of the hypertrophic marker COL-X, akin to the non-coated control hMSCs (Figure 1j). Furthermore, chondrogenic differentiation requires long-term culture (a minimum of 14 days) to express cartilage-specific markers (COL2A1, ACAN, SOX9) [25]. Therefore, the nanoencapsulation process did not significantly impair the viability, proliferation, metabolic activity, and differentiation characteristics of the hMSCs, a key requirement for effective cell therapy. However, it is also important to analyze how these cell-friendly silk nanocoatings act as a protective armour when administered in an inflammatory, hypoxic, protease-rich, oxidative OA niche.

3.2 | Ionomer Shells Shielded hMSCs Against Catabolic and Biomechanical Stressors of the Knee Joint

3.2.1 | Catabolic Stress

The OA milieu in the knee joint in vivo is comprised of a combination of microenvironmental stressors. This includes pro-inflammatory cytokines (IL-1β, TNFα, IL-6) secreted by the M1 macrophages and inflamed synovial fibroblasts, oxidative stress generating reactive oxygen species (ROS), proteases released by the pro-arthritic chondrocytes and the overall hypoxic microenvironment of hyaline cartilage [52, 53]. Therefore, any cells delivered to the osteoarthritic knee joint may enter senescence or undergo complete apoptosis, rendering the 'cellular therapy' options futile. Hence, to achieve an efficient outcome with stem cell therapy, the hMSCs must be viable, proliferate and avoid apoptotic outcomes due to the influence of the inflammatory OA niche. The shielding effect of the nanoencapsulation against these stressors was evaluated by mimicking the OA-like conditions in vitro using a combination of chemicals and cytokines (Figure 2a).

3.2.1.1 | Inflammation. Inflammation plays a key role in the progression of OA, characterized by an increased release of pro-inflammatory cytokines and chemokines. Post-incubation in an in vitro inflammatory stress medium, the nanocoated cells demonstrated enhanced cell viability compared to the non-coated control (Figure S8). The 6-bilayer nanoencapsulated cells demonstrated enhanced cell viability (Figure 2b; Figure S10), and lower LDH release (Figure 2c; Figure S11) compared to the 3-bilayer and the non-coated control. Therefore, the 6-bilayer coating effectively demonstrated a barrier effect against the infiltration of inflammatory macromolecules, thereby inhibiting progression toward apoptosis, a crucial checkpoint for successful cell therapy.

3.2.1.2 | Proteases. Degeneration of the articular cartilage extracellular matrix by the protease secretome of native articular chondrocytes is central to the aetiology of OA [53]. Additionally, as the ionomer coatings on the cells comprise the SF coating, it is also important to evaluate the stability and the protective nature of the nanocoatings against proteolytic stress. The nano-encapsulated cells (3 and 6-bilayer) displayed improved cell viability across both concentrations compared to the non-coated controls (Figure S8). Among the nanoencapsulated groups, the 6-bilayer-coated hMSCs displayed increased % cell viability (cell proliferation) (Figure 2b; Figure S10), and membrane integrity (Figure 2c; Figure S11) compared to the 3-bilayer-coated cells. Therefore, deposition of more ionomer layers on the cell surface enhanced barrier protection from proteolytic stress, presumably due to the more resilient protective layer delaying the proteolytic degradation and dissipation of the ionomer shells.

3.2.1.3 | Oxidative Stress. Oxidative stress plays a significant role in the pathophysiology of knee OA, marked by a disproportionate increase in the production of ROS [54] causing significant damage to the cell membrane, lipoproteins, and intracellular nucleic acids. Thus, when stem cells are delivered into an OA microenvironment, they must withstand the oxidative stress and further differentiate into chondrocytes without undergoing senescence or apoptosis. The 6-bilayer coating efficiently preserved the viability of the stem cells, more so than the 3-bilayer and the non-coated cells, even when primed with 500 µM of H_2O_2 (Figure S8). A similar trend was also observed for cellular proliferation and LDH release in the 6-bilayer system compared to the 3-bilayer and non-coated controls in the 500 µM oxidative stress medium, indicating elevated % living cells (Figure 2b; Figure S10) with strong cell membrane integrity (Figure 2c; Figure S11). Therefore, nano-encapsulation protected the stem cells from senescence and subsequent apoptosis caused by oxidative stress, which is essential for successful cartilage regeneration in degenerated tissues.

3.2.1.4 | Hypoxia. Hypoxia is a direct catabolic regulator in OA pathogenesis through the active secretion of pro-inflammatory chemokines, cyclooxygenase 2 (Cox2), and prostaglandins, facilitated by signaling crosstalk with the inflammatory Nuclear factor kappa B (NF-κB) pathway, as well as promoting metabolism and ECM secretion during chondrogenesis [55, 56, 57]. Therefore, nanoencapsulation should safeguard the cells from hypoxia-induced cell death and subsequently promote healthy cell survival, proliferation and differentiation. The non-coated hMSCs demonstrated almost no survival and decreased viability in the hypoxic microenvironment (Figure 2b,c), as validated by the abundance of dead cells (Figure S9), relatively low % cell viability (Figure S10), and increased LDH release, indicating loss of membrane integrity (Figure S11). In contrast, the nano-encapsulated hMSCs demonstrated a higher survival rate with increased cellular proliferation (increased % cell viability) (Figure 2b; Figure S10) and lower apoptosis (Figure 2c; Figure S11) with 6-bilayer displaying better advantage over 3-bilayers. Thus, increased ionomer shell layers successfully inhibited the diffusion of cobalt chloride from the surrounding culture media into the cells to induce hypoxia-induced cell death, thus effectively demonstrating barrier-function against microenvironmental stress.

3.2.1.5 | Cocktail (Inflammation + Protease + Oxidative Stress + Hypoxia). In vivo OA knee joint microenvironment is a blend of inflammation by cytokines and chemokines, ROS, secreted matrix proteases and an extremely hypoxic microenvironment. When the nano-encapsulated hMSCs were primed with the in vitro cocktail stress media conditions for 72 h, the 6-bilayer coating demonstrated superior protective functions compared to the 3-bilayer and non-coated control cells. This result included significantly improved cell viability (Figure 2d),

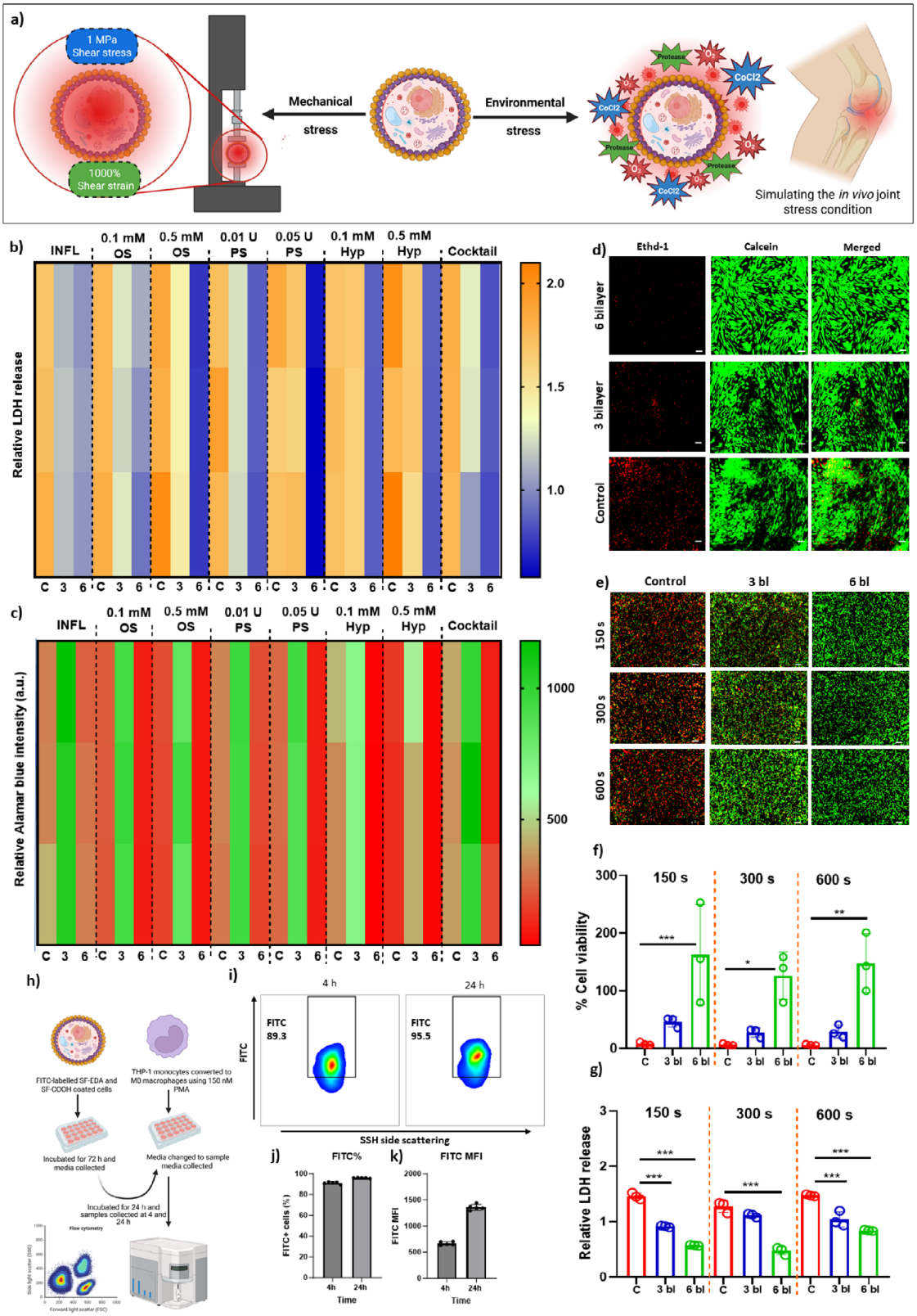

FIGURE 2 | The protective role of increasing layer thickness in shielding the coated hMSCs against OA microenvironmental and biomechanical stressors, (a) Graphical representation of the experimental overview to evaluate the efficacy of nanocoating strategies in protecting the cell against OA stress signals, (b) Heat map representing the LDH release profile of the 3 and 6-bilayer coated hMSCs post 72 h incubation in OA-mimicking catabolic stress media *(INFL: Inflammation media, OS: Oxidative stress media, PS: Protease stress media, Hyp: Hypoxia stress media)*, (c) Heat map representing the Alamar blue intensity profile of the 3 and 6-bilayer coated hMSCs post 72 h incubation in OA-mimicking catabolic stress media, (d) Live/dead micrographs showing the viability of nano-encapsulated hMSCs incubated in 72 h cocktail stress media (Combination of 0.05 ng/mL of IL-1β, 0.05 ng/mL of TNFα and 0.1 ng/mL of IL-6), 0.5 mM of H_2O_2, 0.05 U of Protease XIV and 0.5 mM of $CoCl_2$) (Scale bar: 100 μm), (e) Live/dead micrographs

enhanced cell viability (cell proliferation) (Figure 2b; Figure S10), and a decreased tendency toward apoptosis as a function of loss of membrane integrity, measured using the LDH assay (Figure 2c; Figure S11). Thus, the increase in ionomer shell layers around the cells subsequently protected the cells from severe OA microenvironmental stress by resisting proteolytic degradation for 72 h and limiting the diffusion of catabolic stressors into the cells, thereby preventing cellular apoptosis.

3.2.2 | Biomechanical Stress

The knee joint in the human body is subjected to constant mechanical loading, serving as a crucial element of the human locomotion system [58]. There is an increased prevalence of shear strain over compressive strain at the osteochondral interface, making it a significant indicator of the mechanobiological response of resident cells to surrounding shear stimuli [59, 60]. Thus, the transplanted cells must adapt to the mechanical stimuli in the knee joint without impairing cell viability (Figure 2a). The 6-bilayer nanocoating preserved the viability of the hMSCs after being subjected to mechanical stress for 150, 300, and 600 s, respectively, compared to the 3-bilayer and non-coated controls (Figure 2e). This was further observed in the significant increase in % cell viability (as a function of cell proliferation) in the 6-bilayer nanoencapsulated hMSCs compared to the non-coated and 3-bilayer nanocoated cells. (Figure 2f). The loss in membrane integrity measured as a function of LDH release was also minimized in the encapsulated groups for all experimental conditions compared to the non-coated control, with the 6-bilayer overpowering the 3-bilayer group (Figure 2g). Therefore, the strong persistence of the silk ionomer nanoencapsulation around the cells for 72 h, along with its delayed dissipation and increased bilayers, acted as a mechano-resilient barrier against shear conditions, while maintaining cellular health and membrane integrity.

3.2.3 | Extrusion Shear Stress

During local or intravenous transplantation, cells experience high shear and extensional stresses as they pass through narrow-gauge needles, often leading to membrane rupture, apoptosis, and reduced therapeutic efficacy [61]. Therefore, the purpose of the syringe extrusion experiment was to simulate these mechanical challenges in vitro and determine whether the 3- and 6-bilayer SF-ionomer nanocoatings could preserve cell integrity and viability under clinically relevant flow conditions (32-gauge needle, 150 µL/minute). The Ethd-1 staining post-extrusion of the encapsulated and the non-encapsulated cells demonstrated significant cell death in the non-coated control group, whereas few dead cells were observed in both ionomer-coated groups as shown in Figure S12. Alamar blue quantification (measuring the % cell viability) also revealed elevated % cell viability in the 6-bilayer coated hMSCs (Figure S12). Low shear can influence stem cell differentiation. [62, 63] While polymeric coatings shield the cells from direct shear stress, high-viscosity polymers generally induce elevated shear stress on cells, which can impair cellular integrity and post-transplantation functions [64]. In contrast, these low-concentration SF-multilayer coatings avoided the negative influence of shear stress while maintaining the membrane stability and metabolic activity of the hMSCs.

A major roadblock to stem cell therapy in OA lies in the altered phenotype of chondrogenically differentiated hMSCs, which is caused by the prevalent inflammatory and elevated ROS-rich environment. Therefore, in the current study section, we demonstrated how the LBL nanoencapsulation of hMSCs with silk ionomers provided a combined protective shield against in vitro OA-mimicking catabolic and biomechanical stressors, while also defending against the shear stress generated by injections. Such protection will aid in neo-articular cartilage regeneration when transplanted in an in vivo osteoarthritic knee joint without drifting toward hypertrophic differentiation. Although, the silk ionomer-based hMSC nanoencapsulation did not alter cell functioning while being protective against harsh OA milieu, it is important to assess preliminary in vitro immune responses to these ionomers for future long-term in vivo administration applications.

3.3 | Immune Response Profile and Fate Mapping of Nanocoatings

Silk is an FDA-approved protein biopolymer used for a wide array of tissue engineering applications, ranging from disease modeling to regenerative medicine [65, 66]. This can be attributed to its mechanical properties, biocompatibility, biodegradability, and chemical accessibility [20]. Determining the immunological fate of SF-based biomaterials is challenging due to the multitude of factors (e.g., secondary conformation, molecular weight, purity). SF generally evokes a limited immune response that subsides within a few hours to a few days post-implantation [67, 68]. The chemical modifications of the side chains of SF protein also influence immunogenicity by exposing or masking any potential antigenic epitopes, thereby altering immune cell recognition sites [69]. The positive and negatively charged ionomers used for nanoencapsulation are both chemically modified silk chains at aspartate and glutamate residues (SF-EDA) and tyrosine residues (SF-COOH), respectively [14]. Therefore, the immune response of the nanocoating fragments following disengagement from the cell surface after 72 h, was evaluated. THP-1 ASC reporter cell lines were used for immunological profiling of the silk ionomers based on their inflammasome activation reporter capability, as indicated by green fluorescent protein (GFP)-labelled ASC speck

demonstrating the shielding efficacy of 3 and 6-bilayer nanocoating in protecting the hMSCs from mechanical stress for 150, 300, and 600 s respectively (Scale bar: 100 µm), (f) Quantification of cell viability as a function of cell proliferation after subjecting the nanocoated cells to mechanical stress for 150, 300, and 600 s respectively (*$p < 0.05$, **$p < 0.01$ and ***$p < 0.001$) (normalized to the control and nanoencapsulated cells subjected to no shear force), (g) Evaluation of cell membrane integrity as a function of LDH release quantification after subjecting the nanocoated cells to mechanical stress for 150, 300, and 600 s respectively (*$p < 0.05$, **$p < 0.01$ and ***$p < 0.001$), (h) Experimental work flow to predict the fate of the nanocoatings post-disengaging from the cell surface, and (i,j,k) demonstrating the internalization of the detached silk ionomer by the macrophages using flow cytometry.

formation, observed by fluorescence microscopy [70]. Elevated GFP expression in SF-EDA at 24 and 72 h was observed compared to SF-COOH and SF only, implicating increased ASC-speck formation, possibly due to inflammasome activation comparable to the positive control (LPS) (Figure S13). Inflammasome activation can be further traced downstream through the activation of the inflammatory signaling cascade, leading to the secretion of pro-inflammatory IL-1β and IL-18, as measured by the HEK-IL-1β reporter cell line. When compared to SF, IL-1β secretion demonstrated a significant 2-fold increase ($p < 0.001$) for SF-EDA and a 1.25-fold increase ($p = 0.338$) for SF-COOH at 24 h, which maintained the same IL-1β secretion pattern at 72 h. However, for both SF-EDA and SF-COOH, there was no significant decrease in IL-1β secretion from 24 to 72 h. Therefore, SF-EDA ionomer demonstrated inflammatory characteristics with increased IL-1β secretion and enhanced GFP expression linked to inflammasome-activated ASC speck formation compared to SF-COOH ionomer, which was comparable to unmodified SF. EDA is known to demonstrate inflammatory effects against *Mycobacterium tuberculosis* by promoting M1 polarization of macrophages and the production of pro-inflammatory cytokines through the activation of the p38/MAPK pathway [71]. Hence, there could be two strategies to evade the inflammatory immune response by the SF-EDA ionomer used for nano-encapsulation: (a) rapid clearance once detached from the cell through phagocytosis by the macrophages, or (b) immobilizing a cocktail of anti-inflammatory cytokines into the ionomer bilayers to impair the immune response.

Macrophages play a crucial role in internalizing apoptotic cells and degraded biomaterials within the body, as well as in activating adaptive immune cells post-implantation or following cellular transplantation through phagocytosis [72]. Therefore, it would be interesting at first to examine whether the detached ionomers, which otherwise elicit inflammatory responses (SF-EDA), can be cleared through phagocytosis by macrophages (Figure 2h). Flow cytometry analysis revealed almost 89.3% and 95.5% internalisation of the FITC-labelled SF-EDA within 4 and 24 h, respectively, implying complete clearance of the degraded and detached ionomers (Figure 2i–k). Thus, the rapid clearance could avoid triggering innate immune response within few hours of the transplantation but post internalisation by the phagocytes and presented to the adaptive immune system through the major histocompatibility complex I or II (MHC I/II) receptors, the possibility of triggering cytotoxic T-cell-mediated adaptive immune response can impart a deleterious effect on the overall success of the transplanted cells within the diseased site. Therefore, a more reliable strategy would be to investigate a functionalized anti-inflammatory nanocoating that preserves cellular integrity within a catabolic OA niche, while also imparting immunomodulatory effects into the surrounding inflammatory microenvironment.

3.4 | Immunomodulatory, Anti-Inflammatory Nanocoating Inhibited Hypertrophic Differentiation of the Chondrocytes and Promoted M1 Macrophage Repolarization

Inflammation is an established pathophysiological driver of OA orchestrated by the joint-resident immune cells, synoviocytes and articular chondrocytes [73, 74]. A significant hurdle in hyaline cartilage regeneration lies in the phenotypic drift of the articular chondrocytes toward hypertrophic differentiation with abnormal overexpression of transient cartilage genes (COL-X, MMP1/13, collagen type-I (COL-I), etc.) and downregulation of hyaline cartilage markers [75]. A wide range of tissue engineering strategies has been employed to mitigate chondrocyte hypertrophy by combining different small-molecule regulators of OA and biomaterials, in injectable or implantable form [28, 76, 77]. Therefore, LBL coatings of the chondrocytes with anti-inflammatory cytokine-loaded silk ionomers not only shield the chondrocytes from the inflammatory stress but could also nourish the cells with the anti-inflammatory regulators to transiently attenuate hypertrophic maturation. A preliminary macrophage polarization experiment to assess changes in the inflammatory response of the SF-EDA post-cytokine addition showed a sharp decrease in CD86 marker expression in the mixture of SF-EDA and anti-inflammatory cytokines compared to the SF-EDA only group, demonstrating successful incorporation of the anti-inflammatory effect on the previously observed inflammatory response to the SF-EDA ionomer (Figure S14). Following encapsulation, the 6-bilayer anti-inflammatory nanocoating preserved the viability and proliferation potential of the chondrocytes, as evaluated by live/dead staining and the Alamar Blue assay (Figure S15). The anti-inflammatory ionomer encapsulated chondrocytes, when incubated in hypertrophic inflammatory media (Figure 3c), exhibited a significant reduction in expression of COL-X (Figure 3a,b) and RUNX2 (Figure S16), relative to both ionomer-coated and uncoated controls ($p<0.001$). This suggests that the anti-inflammatory nanocoating delivered sustained trophic support, effectively delaying the onset of hypertrophic differentiation. Autologous chondrocyte implantation (ACI) is considered one of the standard FDA-approved surgical procedures for treating OA, but challenges related to the hypertrophic maturation of the implanted cells lead to insufficient cartilage regeneration within the defect site. In this regard, the current study demonstrated that anti-inflammatory 6-bilayer nanoencapsulation of chondrocytes preserved hyaline cartilage phenotype and prevented cellular senescence under OA-mimicking inflammatory conditions in vitro, thereby advancing the potential of chondrocyte-based cell therapy for OA.

A major pathological driver of OA progression is the infiltration of pro-inflammatory M1 macrophages, further aggravating the inflammatory niche. Therefore, effective regenerative therapies for OA must also actively focus on modulating the local immunological niche to foster a pro-regenerative microenvironment conducive to neo-cartilage formation. The activation of the M1 macrophages by the respective LPS, IFNγ or damage-associated molecular patterns (DAMPs) produced by the degrading articular cartilage tissue, releases a plethora of pro-inflammatory cytokines (IL-1β, IL-6, TNFα) that further contribute to the severity of OA [78]. Thus, when the anti-inflammatory nanocoated chondrocytes were co-cultured with polarised M1 macrophages, they repolarized them to the anti-inflammatory M2 subtype, akin to the in vivo immunomodulation process (Figure 3d). A pilot experiment to evaluate the cytokine combination suitable for M2 polarization demonstrated the superiority of an IL-4, IL-13, and IL-1Ra cocktail in achieving maximum M2 conversion, accompanied by enhanced CD206 expression (Figure S17) [33].After 72 h of co-culture with the pro-inflammatory M1 macrophages, the anti-inflammatory coated chondrocytes repolarized the M1 macrophages to the anti-inflammatory M2 phenotype. This is

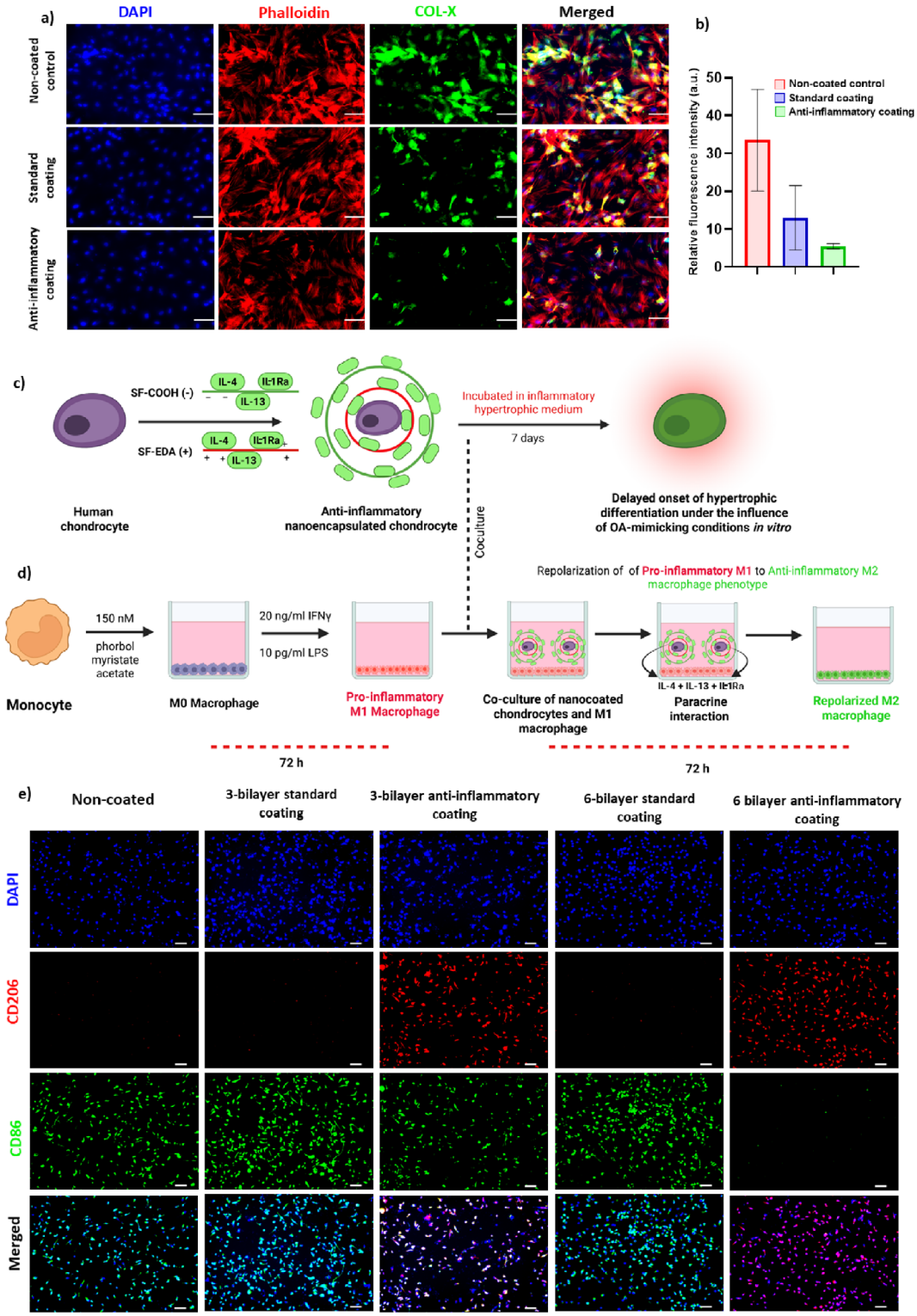

FIGURE 3 | An anti-inflammatory nanocoating to modulate hypertrophic differentiation of chondrocytes and simultaneously immunomodulate the surrounding inflammatory microenvironment, (a) Fluorescence micrographs comparing the expression pattern of hypertrophic marker, collagen type X (COL-X) in the nanocoated chondrocytes post-incubation in hypertrophic medium for 7 days *(anti-inflammatory coating: silk ionomer nanocoating functionalized with anti-inflammatory cytokines, standard coating: cationic and anionic silk ionomer, non-coated control: only hMSCs without encapsulation)* (Scale bar: 100 μm), (b) Corresponding relative COL-X fluorescence intensities of the respective non-coated control, standard coating and anti-inflammatory coating experimental groups, (c) Graphical representation illustrating the effect of anti-inflammatory nanocoating on the hypertrophic differentiation of chondrocytes, (d) Graphical representation of the immunomodulatory effect of the anti-inflammatory nanocoating in promoting M1 repolarization to M2 when co-cultured with anti-inflammatory coated chondrocytes for 72 h, and (e) Fluorescence micrographs comparing the potency of M2 phenotype conversion from M1 post-co culturing with anti-inflammatory nanocoated chondrocytes using M1-specific CD86 and M2-specific CD206 marker expressions (Scale bar: 100 μm).

characterized by upregulation of CD206 expression and downregulation of CD86 expression, compared to the standard ionomer-coated chondrocytes (Figure 3e). Comparative analysis revealed that 6-bilayer encapsulation induced a significantly higher degree of macrophage polarization, as evidenced by a decrease in M1/M2 ratio (0.06), compared to the 3-bilayer system (1.14) (Figure S18), underscoring the enhanced immunomodulatory efficacy conferred by additional bilayers under inflammatory conditions (Figure 3e). Macrophages have emerged as prominent therapeutic targets in OA due to their substantial infiltration and prevalence within inflamed knee joints and the surrounding periarticular tissues [79]. A diverse array of small molecules and extracellular vesicles derived from various cell types has been explored for modulating macrophage function in osteoarthritic joints. This is achieved by favouring M2 polarization from M0 and subsequently inhibiting M1 phenotype conversion, a key parameter for immunomodulatory therapy in managing inflammation in OA [80].

Thus, based on the current findings, it can be inferred that the anti-inflammatory nanocoating represents a significant advancement in regenerative cell therapy for OA management by: (i) preserving cellular proliferation and membrane integrity under catabolic and biomechanical stress conditions, comparable to standard nanoencapsulation; (ii) delaying the onset and progression of hypertrophic differentiation in chondrocytes exposed to an inflammatory hypertrophic milieu; and (iii) exerting immunomodulatory effects through the release of anti-inflammatory cytokines that facilitate the repolarization of M1 macrophages toward the M2 phenotype. Future studies may focus on covalently conjugating immunomodulatory cytokines to chemically modified SF solutions, followed by enzymatic crosslinking, to promote M1-to-M2 macrophage repolarization and assess the long-term stability of the anti-inflammatory M2 phenotype in vitro over extended durations (14–28 days). The native in vivo joint microenvironment during OA comprises an intricate signaling crosstalk between the joint-resident cells (chondrocytes, synoviocytes, and osteoblasts) and the infiltrating immune cells (Natural killer cells, CD8+ T cells and macrophages), releasing a wide array of chemokines, cytokines and ROS. This creates a deleterious cycle of inflammation, oxidative stress and continuous ECM breakdown. In our current study, we aimed to recapitulate the anatomical architecture of the osteoarthritic joint microenvironment in vitro using different cell types, while employing cytokine and chemical cocktails to chemically mimic the physiological effects of OA. This in vitro OA-mimicking niche was utilized in our research to test the efficacy of the barrier function and immunomodulatory activity of the SF-ionomer nanoencapsulated hMSCs and Chondrocytes, targeted for OA attenuation. However, considering the complexity of the native inflammatory joint milieu during OA, future investigations must be aimed at evaluating the shielding efficiency and immune-regulatory profile of the nanocoatings under in vivo conditions. Considering macrophages as an important therapeutic target for OA management, it would be interesting to investigate how LBL nanoencapsulation contributes to advancing immunotherapeutic strategies in OA, extending beyond stem cell and chondrocyte-based interventions to include immune cells, such as macrophages.

3.5 | Macrophage Polarization Driven by Nanoencapsulation Inhibited Synovial Fibroblast Inflammation

Macrophages have been targets of regenerative OA therapies due to their defensive role in phagocytosing incoming foreign particles and presenting them to the adaptive immune system, thereby aiding in orchestrating a multitude of immediate and long-term immune responses within the body [81]. Recently, M2 macrophage-derived exosomes polarized the M1 to M2, significantly reduced M1-specific iNOS expression in a rat OA model using an alginate-hyaluronic acid hydrogel system [82]. Genetic engineering-based macrophage reprogramming by intentionally knocking out the inflammatory TNFα gene and overexpressing the anti-inflammatory IL-4 gene in rat bone marrow-derived macrophages demonstrated a consistent immunomodulatory effect against the inflammatory FLS and chondrocytes [8]. Consequently, challenges such as the requirement for ex vivo polarization of M0 to M2 macrophages before administration, the instability and loss of cellular integrity of the M2 phenotype under inflammatory stress, and the use of sophisticated genetic engineering techniques for permanent macrophage reprogramming (e.g., gene insertion or knockout) limit the translational potential of macrophages as an immunotherapeutic tool for OA. Therefore, in the current study, the dual advantage of nanoencapsulation in macrophage-based immunotherapy is demonstrated by conserving cellular integrity under inflammatory stress, while also enabling in situ polarization toward the respective M1 and M2 subtypes based on the immobilized cytokines within the coating bilayers. This finding represents a new path forward in developing anti-inflammatory immunotherapeutic strategies for OA.

Prior to encapsulation, the silk ionomers were immobilized with M1- and M2-specific cytokines, respectively, known to promote the ex vivo polarization of the neutral M0 to M1 and M2 subclasses when added exogenously to the culture medium, respectively (Figure S17). Accordingly, encapsulating the M0 macrophages with cytokine-loaded silk ionomers resulted in the successful polarization of these cells into either the classically activated M1 or alternatively activated M2 subtypes after 72 h (Figure 4a). The primary mechanism behind the entrapment of cytokines into the ionomers is likely due to electrostatic interactions between the charged SF solutions (SF-EDA and SF-COOH) and the cationic and anionic amino acid residues of the cytokines, resulting in non-covalent ionic interactions, supplemented by hydrogen bonding and hydrophobic interactions. Comparable expression of CD86, iNOS (M1) (Figure 4b) and CD206, Arg (M2) (Figure 4c) between the ex vivo polarized and coating-directed polarized macrophages underlines the efficiency of in situ polarization of the nanocoated M0 macrophages, while simultaneously preserving their viability under inflammatory stress (Figure S19). Also, standard (cytokine-free) coatings produced only a mild, transient M1-skewed response, consistent with the expected surface charge effect of cationic polymers (Figure S20). Embedding anti-inflammatory cytokines (IL-4, IL-13, IL-1Ra) within the coatings, however, actively directed macrophage polarization toward the M2 phenotype. This further confirmed the immunomodulatory behaviour was from the cytokine incorporation rather than

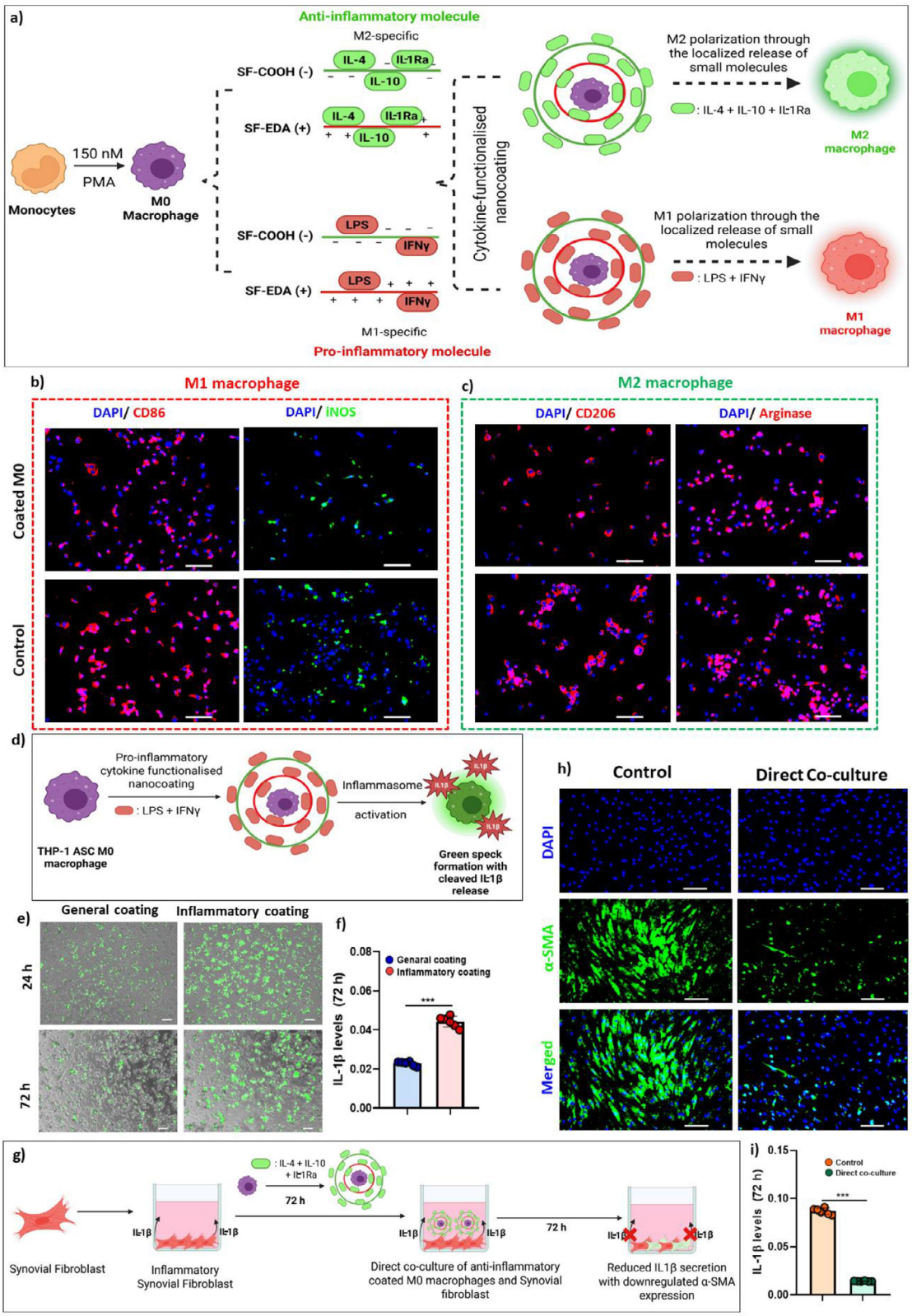

FIGURE 4 | In situ nanocoating-mediated polarization of neutral M0 macrophages to M1 or M2 phenotype and their immunoregulatory role in modulating inflamed OA synovium, (a) Graphical overview of utilizing anti-inflammatory (IL-4 + IL-13 + IL-1Ra) and pro-inflammatory (LPS + IFNγ) cytokine-functionalized nanocoating in promoting M1 and M2 polarization, (b) Fluorescence micrographs confirming the in situ differentiation of M0 macrophages to M1 subtype through CD86 and iNOS protein expression (Scale bar: 100 μm). (c) Fluorescence micrographs confirming the in situ differentiation of M0 macrophages to M2 subtype through CD206 and Arg protein expression (Scale bar: 100 μm), (d) Graphical representation illustrating the differentiation of THP-1 ASC-derived M0 macrophage to M1 phenotype through the pro-inflammatory cytokine-embedded nanocoating, (e) Fluorescence micrographs demonstrating green speck formation within the THP-1 ASC derived macrophages upon inflammatory nanocoating (Scale

the coating material itself. The efficacy of nanoencapsulation-mediated polarization was further assessed on the THP-1 ASC reporter cell line-derived macrophages (Figure 4d). It is observed that the inflammatory cytokine-embedded silk ionomer-coated macrophages demonstrated enhanced green fluorescence compared to the standard-coated macrophages (Figure 4e), followed by a significant increase in IL-1β secretion (2-fold; $p < 0.001$) (Figure 4f). Therefore, the inflammatory nanocoating induced the polarization of M0 to M1 phenotype by activating major inflammatory pathways, resulting in inflammasome activation and increased IL-1β production. Such an inflammatory cytokine-embedded nanoencapsulated macrophage with an M1 polarization tendency could find utility in immunotherapy for various malignancies that result from grade-III OA (e.g., prostate, lung, liver, skin) [83].

A successful macrophage-based immunotherapy in a degenerating OA microenvironment involves the polarization and stable maintenance of M2 plasticity, as well as exerting an anti-inflammatory influence on the surrounding inflamed tissues. One such adversity in an OA niche is the synovial inflammation or synovitis. It is a direct physiological manifestation of knee OA, contributing to the clinical symptoms of joint swelling and inflammatory pain [84]. The secreted catabolic factors by the inflamed synovial tissue stimulate cartilage ECM degradation, disrupting hyaline cartilage homeostasis. Therefore, the anti-inflammatory nanoencapsulation on the macrophages should be able to deploy an immunomodulatory effect by inhibiting the production of inflammatory cytokines by the FLS (Figure 4g). Hence, the neutral M0 macrophages, after encapsulation with anti-inflammatory cytokine-immobilised nanocoatings and co-cultured with already inflamed FLS for 72 h, showed a significant reduction in IL-1β production (eight fold; $p<0.001$) (Figure 4h) and a decrease in α-SMA expression (Figure 4i; Figure S21). An enhanced level of α-SMA expression, a key myofibroblast marker, has been observed in the synovial fluid of post-traumatic OA patients [85]. Thus, a reduction in α-SMA expression in the FLS signifies a reduced tendency toward fibrosis, which is considered a pathophysiological driver of OA progression [86].

A monocyte-based immunotherapy requires a two-step ex vivo polarization process, with an initial differentiation into adherent M0 macrophages, followed by polarization into the M2 subtype to exhibit an anti-inflammatory effect. While the present study did not include a direct co-culture model with M1 macrophages, our data indirectly addressed this question by testing the nanocoated cells under controlled exposure to key M1-associated stressors, including inflammatory cytokines, proteases, and oxidative stress inducers, characteristic of the OA joint microenvironment [87]. Under these conditions, the 6-bilayer SF-ionomer coating effectively preserved cell viability, proliferation, and membrane integrity compared with the 3-bilayer and non-coated controls, demonstrating substantial resistance to the deleterious factors secreted by M1 macrophages. These results support the protective and stabilizing role of the nanocoating even in an inflammatory milieu.

The next plausible strategy for improving the retention, barrier function and immunomodulatory function of the nanocoating strategy could be investigated upon transition from single cells to 3D spheroids. Enhanced electrostatic interactions between the cationic ionomers and negatively charged cell membranes could be exploited to slow degradation of the nanocoatings.

3.6 | 3D Spheroids Exhibited Superior Nanocoating Retention Than Single Cells With Effective Immune Evasion

With the recent advances in cell therapy, a paradigm shift has been observed from the delivery of single-cell suspensions to the transplantation of 3D spheroids at diseased sites [88]. The shift is mainly due to the superior in vivo stability of the spheroids, driven by the secretion of ECM proteins (e.g., collagen, fibronectin) that form a physiological barrier around the cells [89]. However, when transplanted into an inflammatory microenvironment, the cells in the outer layer of the spheroid are subjected to apoptosis and immunological attacks by the infiltrating immune cells [90]. In such a case, a cytocompatible nanoencapsulation strategy would temporarily shield the spheroids from the surrounding harsh microenvironment, without affecting cellular proliferation and membrane integrity, while also protecting the spheroids from attack by immune cells (Figure 5a). The 24 h fluorescence microscopy images of 10 000 cells/mL spheroids demonstrated homogeneous deposition of FITC-labelled silk ionomers on the surface (Figure 5b). The confocal images display a dense FITC expression for both spheroid sizes, which gradually decreased, as observed in the 168 h images, illustrating the degradation of the nanocoatings. When comparing 10 000 and 20 000 spheroids at 168 h, the retention of the nanocoating in the 20 000 spheroids was higher than in the 10 000 spheroids, demonstrating the role of size and cell density on nanoencapsulation stability (Figure 5c). Additionally, when measuring the FITC intensities of the nanocoated single cells and spheroids from the culture media at different time points, the intensities in the media samples of the single cell suspensions were higher than those of the spheroids. This signifies a comparatively higher degradation rate of the nanocoating on the single cells than on spheroids. When comparing the results based on cell densities, the FITC intensity was 2-fold higher ($p = 0.002$) in a 20 000 single-cell suspension than in the 20 000 cells/mL spheroid at day 3, a difference that remained constant through day 7 ($p < 0.001$) (Figure 5d). When the FITC intensity of the media samples was estimated within individual spheroid groups for different time-points, there was no significant increase in the relative

bar: 100 μm), (f) Quantification of cleaved IL-1β from the THP-1 ASC-derived M1 macrophages post 72 h inflammatory nanocoating (*$p < 0.05$, **$p < 0.01$ and ***$p < 0.001$), (g) Graphical representation demonstrating the immunomodulatory effect of anti-inflammatory coated macrophages on the surrounding inflamed synovium, (h) Fluorescence micrographs depicting the reduction in α-SMA expression after direct co-culturing the anti-inflammatory coated macrophages with the inflamed synovial fibroblasts for 72 h (Scale bar: 100 μm), and (i) Quantification of cleaved IL-1β from the inflamed synovial fibroblasts post 72 h co-culture with anti-inflammatory coated macrophages (*$p < 0.05$, **$p < 0.01$ and ***$p < 0.001$).

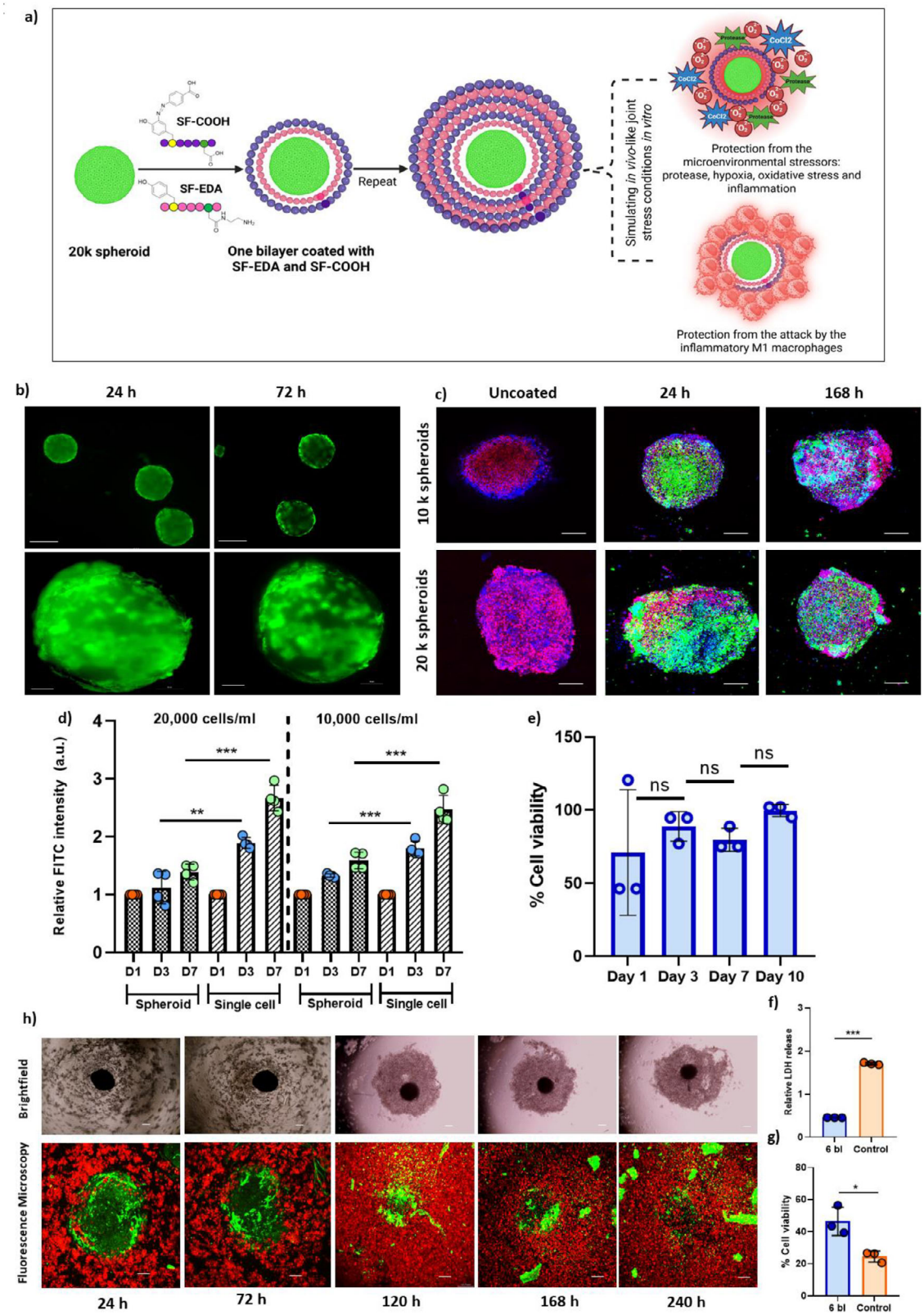

FIGURE 5 | Increased stability of the nanocoating on the surface of 3D spheroids protected the 3D cellular aggregates from immune surveillance. (a) Graphical representation of the deposition of multi-layer cationic and anionic silk ionomers on the surface of 3D spheroids and their subsequent protection of OA microenvironmental stress and attack by the infiltrating M1 macrophages, (b) Representative fluorescence micrographs of FITC-labelled nanocoated 20 000 cells/mL cell spheroid at 24 and 72 h time-points respectively (Scale bar: 200 μm), (c) Confocal fluorescence micrographs comparing the stability of the nanocoatings on the surface of the 3D spheroids at 24 and 168 h time points for both 10 000 and 20 000 cells/mL spheroids (Blue: DAPI, red: Phalloidin and green: FITC-labelled silk ionomer coating) (Scale bar: 100 μm), (d) A semi-empirical quantification to compare the degradation profile of the nanocoatings between single cell and spheroids by measuring the FITC intensities of the detached FITC-labelled ionomers at days 1, 3 and

FITC intensity between days 1 and 3 and days 3 and 7 for 20 000 cells/mL spheroid. Collectively, from these preliminary findings, it can be concluded that: (a) the nanoencapsulation stability of the 6-bilayer was higher in spheroids than for the single cell suspensions, and (b) 20 000 cells/mL spheroids have a higher nanocoating retention capacity than 10 000 cells/mL spheroids. A possible reason for increased coating stability in spheroids could be the stronger electrostatic interactions between the negatively charged ECM proteins (collagen and fibronectin) on the spheroid surface and the positively charged SF-EDA ionomer. Additionally, the lower surface curvature and reduced shear sensitivity, due to the compact 3D structure of the spheroid, possibly improved coating retention during handling.

Further studies with nanocoated spheroids were conducted using spheroids with only 20 000 cells/mL due to their higher coating retention capacity. The 6-bilayer nanoencapsulation did not significantly alter the proliferation potential of the hMSCs within the spheroid, monitored until day 10 (Figure 5e). With the potential application of nanocoated spheroids in OA management, the 6-bilayer encapsulated spheroids preserved the cellular viability (Figure 5f) of the spheroids without indicating any inclination toward apoptosis (Figure 5g) when exposed to joint microenvironmental stressors. This further validates their critical role in further studies related to cell therapy in OA. However, it is also equally important to assess if there is any direct correlation between higher coating retention and improved barrier function of the nanoencapsulated hMSC spheroids.

Therefore, the next objective was to analyze the immune surveillance of M1 macrophages on nanoencapsulated hMSC spheroids, which mimic the in vivo immunological niche in OA. From Figure 5h, it was observed that the 6-bilayer nanoencapsulation shielded the infiltration of M1 macrophages into the 3D spheroid system for up to 72 h, as the coating was intact on the spheroid surface. However, beyond 72 h, the progressive loss of the silk ionomer coating directly influenced the extensive infiltration of macrophages, which continued up to day 10, when the spheroid was fully covered by macrophages (coating had fully degraded). This immunological landscape is similar to the natural immune response pattern during inflammation. This process begins with the initial infiltration of monocytes, which phagocytose cellular debris. This is followed by the recruitment of M1 macrophages to activate acute inflammatory cascades and ultimately re-polarize them into M2, initiating healing and repair [81, 91]. Therefore, the findings reported here illustrated that the nanoencapsulation safeguarded the spheroids from the initial inflammatory immune cell attack until 72 h, until the nanocoating persisted beyond which, the hMSC spheroids exert an immunomodulatory influence to re-polarize the M1 to a healing M2 phenotype that, in turn, infiltrates the chondrogenic hMSC spheroid and could then aid in cartilage regeneration, as previously described [9].

Although the nanoencapsulation safeguarded the 3D spheroids from initial immune surveillance, the ionomer shells began to dissipate after 72 h. Hence, a more advanced strategy is warranted by chemically modifying the cationic ionomer with a functional moiety to facilitate additional covalent interactions on the cell surface beyond electrostatic interactions, thereby increasing the stability of the nanocoatings.

3.7 | Co-Functionalization of EDA and TA Onto SF Strengthened the Structural Stability of the Nanocoatings Through Additional Di-Tyrosine Linkage

Earlier findings from our study demonstrated that the 6-bilayer nanoencapsulation stayed stable on the cell surface for 72 h. Beyond this period, the coating is dispersed from the cell surface and is generally phagocytosed by circulating macrophages within 24 h. However, in certain inflammatory disorders like cardiovascular diseases, type II diabetes, or grade IV OA, the transplanted cells require a long-term defense system to preserve viability and function. Therefore, developing a nanoencapsulation system with enhanced stability on the cell surface without compromising viability is desirable for efficient cell therapy application involving immunomodulation and tissue repair. Co-functionalizing tyramine (TA) to the silk chain, along with EDA, can increase the number of tyrosine units while retaining the net positive charge, which is essential for nanocoating [37, 92]. Further, an increase in tyrosine units in SF biopolymer can enhance the possibility of increased di-tyrosine crosslinking during HRP-assisted gelation. It can further facilitate the phenolic crosslinking between the TA group in the ionomer and the phenolic residues present on the cell surface receptors and peri-cellular matrix in the presence of HRP and H_2O_2, in addition to the electrostatic interactions (Figure 6a) [37, 93, 94]. Such supplementation of covalent crosslinking, along with the electrostatic interactions, should enhance coating stability by further delaying degradation and detachment of the ionomer shells.

The incorporation of TA into the SF-EDA ionomer has been confirmed through various analytical methods. ^{1}H NMR spectroscopy confirmed the covalent incorporation of EDA and TA to the silk chains. The methylene protons due to EDA appeared next to the Tyr β proton peaks of SF (chemical shift 2.5–3.5 ppm) on the NMR spectrum (Figure S22) [14]. Similarly, the aromatic proton peaks of TA appeared in similar chemical shifts (6.7–7.05 ppm) of SF tyrosine residues (Figures S23 and S24) [14, 22]. Molecular weight estimation using ImageJ software following PAGE analysis demonstrated an increase in the mean molecular weight of the SF-EDA-TA to 77.5 kDa from 73 kDa (only SF-EDA),

7 (*$p < 0.05$, **$p < 0.01$ and ***$p < 0.001$), (e) Quantification of % cell viability as a function of cell proliferation within the 3D spheroids post 6-bilayer encapsulation up to day 10 using alamar blue assay (*$p < 0.05$, **$p < 0.01$ and ***$p < 0.001$) (normalized to non-coated 3D spheroids), Quantification of (f) LDH release and (g) % cell viability of the 6-bilayer nanoencapsulated 3D spheroids post 72 h incubation in cocktail stress media (*$p < 0.05$, **$p < 0.01$ and ***$p < 0.001$) (normalized to non-coated 3D spheroids not exposed to cocktail OA stress), and (h) Bright-field and fluorescence microscopy images highlighting the shielding effect of the nanocoating in preventing the M1 macrophage infiltration up to 72 h (Scale bar: 100 μm).

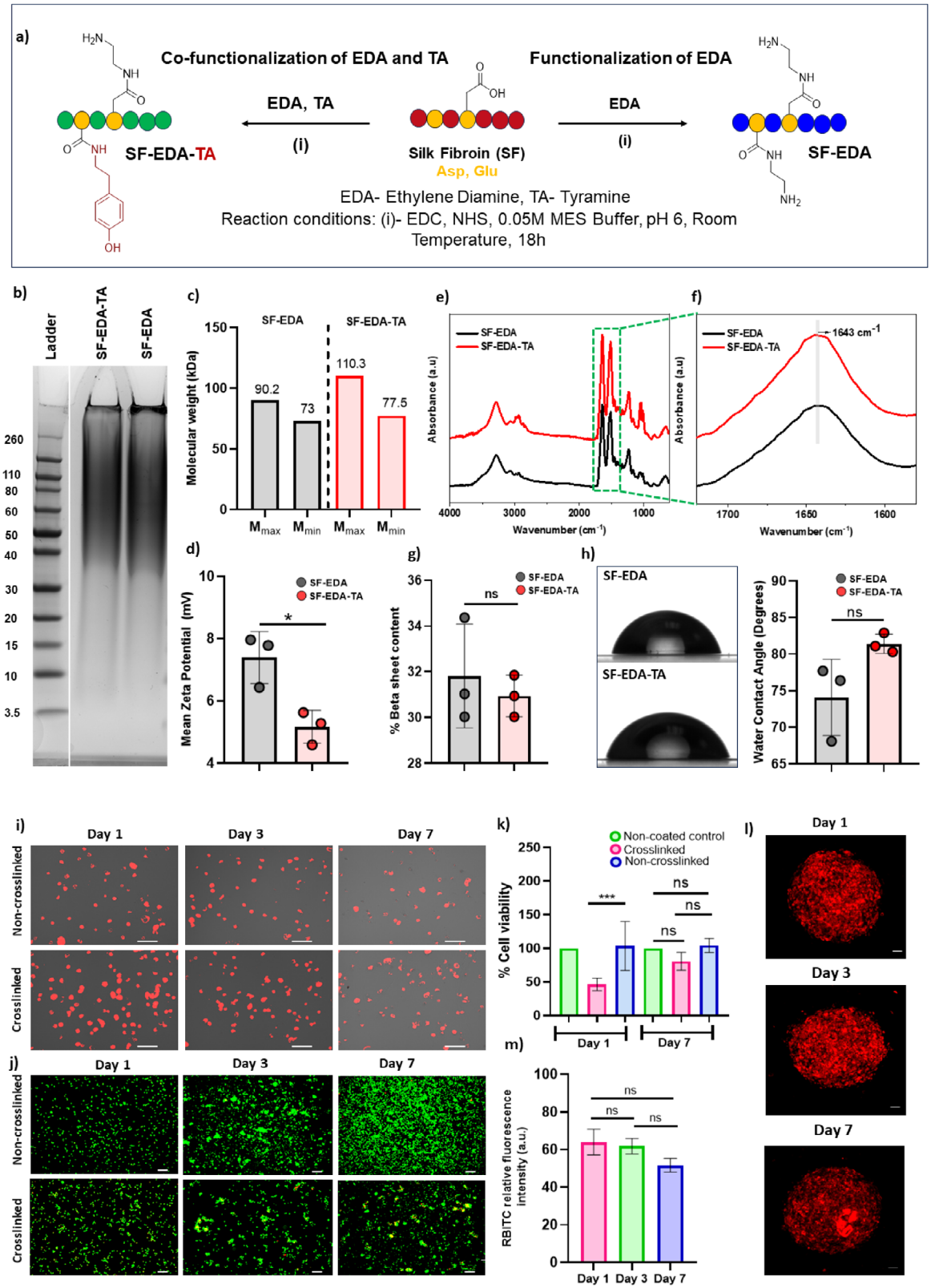

FIGURE 6 | Co-functionalization of tyramine (TA) along with EDA directly into the silk chain increased the stability of the nanocoating on the cell surface due to additional covalent interaction. (a) Chemical synthesis of SF-EDA and SF-EDA-TA using carbodiimide coupling chemistry, (b) Polyacrylamide gel image of SF-EDA and SF-EDA-TA with reference protein ladder, (c) Quantification of mean and maximum molecular weight after co-functionalization of TA and EDA into the silk chains, (d) Zeta potential measurements to estimate the change in overall charge of SF-EDA post-incorporation of TA into the silk chains (*$p < 0.05$, **$p < 0.01$ and ***$p < 0.001$), (e,f,g) FTIR measurements to quantify the alteration in beta sheet content post co-functionalization of TA into the cationic silk ionomer (*$p < 0.05$, **$p < 0.01$ and ***$p < 0.001$), (h) Water Contact Angle (WCA) measurements of SF-EDA and SF-EDA-TA (*$p < 0.05$, **$p < 0.01$ and ***$p < 0.001$), (i) Fluorescence micrographs to compare the stability of the

indicating successful incorporation of tyramine groups into the SF-EDA ionomer (Figure 6b,c; Figure S25). The incorporation of TA was further confirmed by the decrease in the zeta potential of the SF-EDA from 7.39 to 5.16 mV in the SF-EDA-TA, indicating the reduction in the positive amine groups due to the substitution of TA moieties into the silk chain (Figure 6d). However, no significant difference in the percentage of beta sheet content of both SF-EDA (31.81%) and SF-EDA-TA (30.84%) was observed upon FTIR spectra quantification (Figure 6e,f), implying no significant changes in secondary structure conformation post-modification with TA (Figure 6g). Water contact angle (WCA) measurements showed an increase in the hydrophobicity of the SF-EDA-TA biopolymer, with a water contact angle of $81.43^{\circ} \pm 1.09^{\circ}$ compared to SF-EDA ($74.07^{\circ} \pm 4.25^{\circ}$) (Figure 6h). Taken together, it can be concluded that the successful co-functionalization of TA and EDA onto SF resulted in the development of SF-EDA-TA ionomer.

Fluorescence microscopic images confirmed the coating stability up to day 7 for both the crosslinked and the non-crosslinked (control) group. When compared, the crosslinked group showing enhanced stability, possibly due to oxidative phenolic crosslink formations between the tyrosine units of SF-EDA-TA (Figure 6i). A similar stability profile of the SF-EDA-TA ionomer nanocoating was observed for THP-1 immune cells, due to the covalent interaction that extends beyond the interaction between the cell surface and pericellular matrix phenolic groups and TA residues in situ (Figure S26). Live/dead imaging of the nanoencapsulated cells (crosslinked and non-crosslinked) at days 1, 3, and 7 showed that the SF-EDA-TA nanocoating was cytocompatible (Figure 6j; Figure S26). However, a decrease in cellular proliferation was observed within 24 h of incubation in the crosslinked SF-EDA-TA nanocoating, which subsequently increased at day 7, compared to the non-coated and non-crosslinked (only SF-EDA-TA) controls, respectively (Figure 6k). This can be attributed to the oxidative stress-induced cell death caused by excess secretion of reactive oxygen species due to the direct exposure of H_2O_2 to the cells [95, 96]. Additionally, when the RBITC-labelled SF-EDA-TA nanoencapsulated hMSCs were seeded on a 96 U-bottom plate at a density of 20 000 cells/mL, the nanocoated cells successfully formed spheroids and retained their coating until day 7 (Figure 6l,m). Thus, the covalent phenolic crosslinking stabilized the nanoencapsulation, even in 3D spheroids, beyond single-cell suspensions, ensuring the activation of intercellular signaling cascades required for cellular aggregation and spheroid formation [97].

Cell surface engineering has been widely explored to introduce a wide range of chemical interactions between cell surface functional groups and binding sites with biomaterials, thereby influencing mechanotransduction and cell differentiation [98]. Therefore, the development of tunable cytocompatible nanoencapsulation strategies leveraging the in situ covalent di-tyrosine crosslinking mechanisms offers a new option for more persistent nanocoatings. The on-cell phenolic crosslinking chemistry and the electrostatic interaction between the positively charged ionomer and the negatively charged cell membrane increased the structural stability of the nanoencapsulation from 72 to 168 h (7 days) without compromising cellular integrity. This cell encapsulation strategy, by introducing an additional interaction domain to the ionomers, could be deployed for treating acute inflammatory conditions where the transplanted cells require longer-term protection from hostile environmental conditions and immunological surveillance. The physicochemical properties of the nanocoating can be further tailored by adjusting the concentration and stoichiometric ratio of EDA and TA to control the degree of substitution, crosslinking, hydrophobicity, and charge. This can either aid in delaying or accelerating the degradation of the nanocoating, thereby exhibiting modular characteristics. Ongoing efforts could evaluate the shielding efficacy of the additional covalent crosslinking when the nanocoated cells are subjected to extreme catabolic factors, biomechanical stress and inflammatory immune cell attack. However, it can be hypothesized that the di-tyrosine bond formation with the oxidative coupling of SF tyrosine and phenolic side chains of tyramine should provide a longer-term immunomodulatory effect through the sustained release of the immobilized cytokines into the surrounding niche.

Therefore, the current study focuses on the early post-transplantation phase, where the transplanted cells encounter intense oxidative, inflammatory, and proteolytic stress. The goal of our silk ionomer nanoencapsulation strategy is to provide transient cytoprotection and immune modulation during this critical window, rather than long-term mechanical reinforcement. In vitro, the base cationic-anionic coatings remain intact for ~72 h through electrostatic attraction; the incorporation of tyramine (TA) moieties extends stability to ~168 h via covalent di-tyrosine crosslinking. This 1-week protection aligns with the acute inflammatory phase following implantation, when the majority of transplanted cells are lost. Safely bridging this period markedly improves engraftment and initiates the regenerative cascade. For long-term cartilage repair, the strategy can be further tuned by controlling β-sheet density, covalent crosslinking, and degradation kinetics to extend coating persistence to several weeks.

4 | Conclusions

The current study elucidated the efficacy of an engineered nanoencapsulation approach as a protective cell armour against harsh environmental factors, biomechanical stressors, and shear force, without attenuating the viability, metabolic activity, proliferative potential, and differentiation ability of hMSCs. This work designed an advanced cytokine-functionalized SF-based

TA-functionalized nanocoatings on hMSCs with and without enzymatic crosslinking (Scale bar: 100 μm), (j) Live/dead micrographs of the crosslinked and non-crosslinked TA-functionalized nanocoated hMSCs at days 1, 3 and 7 (Scale bar: 100 μm), (k) Comparing the % cell proliferation rate of the hMSCs post-encapsulation with crosslinked and non-crosslinked TA-functionalized nanocoatings at days 1 and 7 respectively (*$p < 0.05$, **$p < 0.01$ and ***$p < 0.001$) (normalized to non-coated hMSCs), and (l,m) Confocal fluorescence micrographs and RBITC fluorescence intensity demonstrating the stability of the tyramine-functionalized nanocoating on the hMSCs in 3D spheroid platforms (Scale bar: 100 μm) (*$p < 0.05$, **$p < 0.01$ and ***$p < 0.001$).

nanocoating system that successfully exhibited a range of immunomodulatory effects, spanning immune-instructive to immune-regulatory roles. The immune-instructive properties of nano-encapsulation facilitated the coating-mediated polarization of neutral M0 macrophages into M1 or M2 phenotypes. In contrast, the immune-regulatory attributes modulated the repolarization of the M1 macrophages into a healing M2 phenotype, resulting in reduced synovial inflammation. Moreover, the findings also suggest that the nanocoatings exhibit enhanced stability on 3D spheroids compared to single-cell suspensions, with additional activation of a defense system against inflammatory immune surveillance. Lastly, we introduced a new ionomer by incorporating additional covalent interactions (between the cell and the ionomer) beyond electrostatic interactions through the co-substitution of TA and EDA into the silk chains, to delay the degradation of the nanocoatings without affecting cellular homeostasis. Therefore, this study provides a systematic investigation into designing a versatile nanoencapsulation strategy to shield engrafted stem cells, chondrocytes, or macrophages from the deleterious catabolic OA milieu, thereby enabling cartilage repair while simultaneously exhibiting immunomodulatory and immune-instructive effects to initiate healing. In addition, masking the immune recognition sites on the cell surface through nanoencapsulation may also broaden the utility of advancing allogenic cell therapy. This could provide a unique framework for developing clinically feasible regenerative therapies to mitigate OA.

Subsequent investigations may explore the protective potential of these nanocoatings against cell-mediated cytotoxicity through a co-culture setup with various cytotoxic immune cells, including natural killer cells, CD8+ T cells, and dendritic cells. Additionally, follow-up studies can be designed to assess the capacity of these nanocoatings to guide stem cell differentiation in single-cell suspensions or spheroids by sustaining the delivery of differentiation growth factors to the cells. Further co-functionalization of antioxidant small molecules with the silk ionomers would also enable oxidative regulation of the ROS-rich microenvironment, in addition to the already demonstrated immunomodulation. The functionalized nanocoating approach with long-term nanocoating persistence on the cell surface can be further extended to different tissue-specific primary cells. The modular degradability characteristics of the nanoencapsulation strategy can be utilized in managing chronic inflammatory disorders like neural stem cells for neuroinflammation, cardiomyocytes for myocardial infarction, beta cells for type II diabetes and other inflammatory diseases beyond OA.

Acknowledgements

NM acknowledges the Fulbright Nehru Doctoral Research Fellowship 2024–2025 (Grant ID: PS00364933) for providing the opportunity to work as a Visiting Research Scholar at Tufts University, MA. We also thank the NIH for support via P41EB027062 and the National Science Foundation (2104294) for their support of this work. This work was performed in part at the Center for Nanoscale Systems (CNS), a member of the National Nanotechnology Infrastructure Network (NNIN). CNS is part of the Faculty of Arts and Sciences at Harvard University. NM also acknowledges Edward B. Gordon, Brooke Longo, Olivia K. Foster, Ayman Banjar, Merve Turemen Coskun, Liam Harrington Power, Xinxin Li, Kareen A Fajardo Cortes, Derek Ning, and Mariah L. Arral for their valuable help and suggestions in the research work.

Conflicts of Interest

The authors declare no conflicts of interest.

Data Availability Statement

The data that support the findings of this study are available from the corresponding author upon reasonable request.

References

1. C. W. Zeng, "Advancing Spinal Cord Injury Treatment Through Stem Cell Therapy: A Comprehensive Review of Cell Types, Challenges, and Emerging Technologies in Regenerative Medicine," *International Journal of Molecular Sciences* 24 (2023): 14349, https://doi.org/10.3390/ijms241814349.

2. W. Hermann, S. Lambova, and U. Muller-Ladner, "Current Treatment Options for Osteoarthritis," *Current Rheumatology Reviews* 14 (2018): 108–116, https://doi.org/10.2174/1573397113666170829155149.

3. K. Rönn, N. Reischl, E. Gautier, and M. Jacobi, "Current Surgical Treatment of Knee Osteoarthritis," *Arthritis* 2011 (2011): 454873.

4. A. Pirsadeghi, N. Namakkoobi, M. S. Behzadi, et al., "Therapeutic Approaches of Cell Therapy Based on Stem Cells and Terminally Differentiated Cells: Potential and Effectiveness," *Cells & Development* 177 (2024): 203904, https://doi.org/10.1016/j.cdev.2024.203904.

5. C. R. Harrell, B. S. Markovic, C. Fellabaum, A. Arsenijevic, and V. Volarevic, "Mesenchymal Stem Cell-Based Therapy of Osteoarthritis: Current Knowledge and Future Perspectives," *Biomedicine & Pharmacotherapy* 109 (2019): 2318–2326, https://doi.org/10.1016/j.biopha.2018.11.099.

6. S. Loo and N. Wong, "Advantages and challenges of Stem Cell Therapy for Osteoarthritis," *Biomedical Reports* 15 (2021): 67.

7. B. O. Diekman and F. Guilak, "Stem Cell-Based Therapies for Osteoarthritis," *Current Opinion in Rheumatology* 25 (2013): 119–126, https://doi.org/10.1097/BOR.0b013e32835aa28d.

8. C. Liang, S. Wu, G. Xia, et al., "Engineered M2a Macrophages for the Treatment of Osteoarthritis," *Frontiers in Immunology* 13 (2022): 1054938, https://doi.org/10.3389/fimmu.2022.1054938.

9. N. Majumder, S. Roy, A. Sharma, et al., "Assessing the Advantages of 3D Bioprinting and 3D Spheroids in Deciphering the Osteoarthritis Healing Mechanism Using Human Chondrocytes and Polarized Macrophages," *Biomedical Materials* 19 (2024): 025005, https://doi.org/10.1088/1748-605X/ad1d18.

10. A. N. Orekhov, V. A. Orekhova, N. G. Nikiforov, et al., "Monocyte differentiation and Macrophage Polarization," *Vessel Plus* 3 (2019): 10, https://doi.org/10.20517/2574-1209.2019.04.

11. A. Matsuzawa, M. Matsusaki, and M. Akashi, "Effectiveness of Nanometer-Sized Extracellular Matrix Layer-by-Layer Assembled Films for a Cell Membrane Coating Protecting Cells From Physical Stress," *Langmuir* 29 (2013): 7362–7368, https://doi.org/10.1021/la303459v.

12. O. Hasturk, M. J. Rodriguez, J. J. Wheeler, V. Venoor, M. J. Sobkowicz, and D. L. Kaplan, "Silk Nanocoatings of Mammalian Cells for Cytoprotection Against Mechanical Stress," *MRS Bulletin* 46 (2021): 795–806, https://doi.org/10.1557/s43577-021-00114-3.

13. M. De Groot, P. P. M. Keizer, B. J. De Haan, et al., "Microcapsules and Their Ability to Protect Islets Against Cytokine-Mediated Dysfunction," in *Transplantation Proceedings* (Elsevier, 2001), 1711–1712.

14. O. Hasturk, J. K. Sahoo, and D. L. Kaplan, "Synthesis and Characterization of Silk Ionomers for Layer-by-Layer Electrostatic Deposition on Individual Mammalian Cells," *Biomacromolecules* 21 (2020): 2829–2843, https://doi.org/10.1021/acs.biomac.0c00523.

15. U. Kumarasinghe, O. Hasturk, B. Wang, et al., "Impact of Silk-Ionomer Encapsulation on Immune Cell Mechanical Properties and Viability," *ACS Biomaterials Science & Engineering* 10 (2024): 4311–4322, https://doi.org/10.1021/acsbiomaterials.4c00412.

16. U. Kumarasinghe, N. Majumder, J. M. Sutaria, et al., "Temporary Silk Nanocoatings Preserve Immune Cell Functions and Protection Against Biochemical and Mechanical Stressors," *Biomaterials* 325 (2026): 123605, https://doi.org/10.1016/j.biomaterials.2025.123605.

17. B. Wang, O. Hasturk, U. Kumarasinghe, et al., "Temporary Nanoencapsulation of Human Intestinal Organoids Using Silk Ionomers," *Advanced Healthcare Materials* 14 (2025): 2403176, https://doi.org/10.1002/adhm.202403176.

18. M. Hunter, Y. Wang, T. Eubank, C. Baran, P. Nana-Sinkam, and C. Marsh, "Survival of Monocytes and Macrophages and Their Role in Health and Disease," *Frontiers in Bioscience* 14 (2009): 4079, https://doi.org/10.2741/3514.

19. J. Chakraborty, S. Roy, and S. Murab, "Modulation of Macrophage Phenotype, Maturation, and Graft Integration Through Chondroitin Sulfate Cross-Linking to Decellularized Cornea," *ACS Biomaterials Science & Engineering* 5 (2019): 165–179, https://doi.org/10.1021/acsbiomaterials.8b00251.

20. A. R. Murphy and D. L. Kaplan, "Biomedical Applications of Chemically-Modified Silk Fibroin," *Journal of Materials Chemistry* 19 (2009): 6443–6450, https://doi.org/10.1039/b905802h.

21. A. R. Murphy, P. St John, and D. L. Kaplan, "Modification of Silk Fibroin Using Diazonium Coupling Chemistry and the Effects on hMSC Proliferation and Differentiation," *Biomaterials* 29 (2008): 2829–2838, https://doi.org/10.1016/j.biomaterials.2008.03.039.

22. J. K. Sahoo, O. Hasturk, J. Choi, et al., "Sugar Functionalization of Silks With Pathway-Controlled Substitution and Properties," *Advanced Biology* 5 (2021): 2100388, https://doi.org/10.1002/adbi.202100388.

23. D. N. Rockwood, R. C. Preda, T. Yücel, X. Wang, M. L. Lovett, and D. L. Kaplan, "Materials Fabrication From Bombyx Mori Silk Fibroin," *Nature Protocols* 6 (2011): 1612–1631, https://doi.org/10.1038/nprot.2011.379.

24. C. Li, T. Luo, Z. Zheng, A. R. Murphy, X. Wang, and D. L. Kaplan, "Curcumin-Functionalized Silk Materials for Enhancing Adipogenic Differentiation of Bone Marrow-Derived Human Mesenchymal Stem Cells," *Acta Biomaterialia* 11 (2015): 222–232, https://doi.org/10.1016/j.actbio.2014.08.009.

25. N. Majumder, C. Roy, L. Doenges, I. Martin, A. Barbero, and S. Ghosh, "Covalent Conjugation of Small Molecule Inhibitors and Growth Factors to a Silk Fibroin-Derived Bioink to Develop Phenotypically Stable 3D Bioprinted Cartilage," *ACS Applied Materials & Interfaces* 16 (2024): 9925–9943, https://doi.org/10.1021/acsami.3c18903.

26. D. Ghosal, N. Majumder, P. Das, et al., "Enhancing Wound Healing With Sprayable Hydrogel Releasing Multi Metallic Ions: Inspired by the Body's Endogenous Healing Mechanism," *Advanced Healthcare Materials* 13 (2024): 2402024, https://doi.org/10.1002/adhm.202402024.

27. J. Wissemann, A. Heidenreich, H. Zimmermann, et al., "ADP as a Novel Stimulus for NLRP3-Inflammasome Activation in Mice Fails to Translate to Humans," *Purinergic Signalling* 20 (2024): 291–302, https://doi.org/10.1007/s11302-023-09953-y.

28. N. Majumder, S. Seit, N. S. Bhabesh, and S. Ghosh, "An Advanced Bioconjugation Strategy for Covalent Tethering of TGFβ3 With Silk Fibroin Matrices and its Implications in the Chondrogenesis Profile of Human BMSCs and Human Chondrocytes: A Paradigm Shift in Cartilage Tissue Engineering," *Advanced Healthcare Materials* 13 (2024): 2303513, https://doi.org/10.1002/adhm.202303513.

29. L. Dönges, A. DamLe, A. Mainardi, et al., "Engineered Human Osteoarthritic Cartilage Organoids," *Biomaterials* 308 (2024): 122549.

30. L. Wang, F. Zhang, W. Peng, et al., "Preincubation With a Low-Dose Hydrogen Peroxide Enhances Anti-Oxidative Stress Ability of BMSCs," *Journal of Orthopaedic Surgery and Research* 15 (2020): 392, https://doi.org/10.1186/s13018-020-01916-y.

31. M. Kuntjoro, N. Hendrijantini, E. P. Prasetyo, et al., "Cobalt Chloride as a Hypoxia Mimicking Agent Induced HIF-1α and mTOR Expressions of Human Umbilical Cord Mesenchymal Stem Cells," *Pesquisa Brasileira em Odontopediatria e Clínica Integrada* 24 (2024): 220128, https://doi.org/10.1590/pboci.2024.020.

32. K. Shang, J. Rnjak-Kovacina, Y. Lin, R. S. Hayden, H. Tao, and D. L. Kaplan, "Accelerated In Vitro Degradation of Optically Clear Low β -Sheet Silk Films by Enzyme-Mediated Pretreatment," *Translational Vision Science & Technology* 2 (2013): 2–2, https://doi.org/10.1167/tvst.2.3.2.

33. S. Roy, A. Sharma, and S. Ghosh, "Macrophage Polarization Profiling on Native and Regenerated Silk Biomaterials," *ACS Biomaterials Science & Engineering* 8 (2022): 659–671, https://doi.org/10.1021/acsbiomaterials.1c01432.

34. R. M. Stefani, S. S. Halder, E. G. Estell, et al., "A Functional Tissue-Engineered Synovium Model to Study Osteoarthritis Progression and Treatment," *Tissue Engineering Part A* 25 (2019): 538–553, https://doi.org/10.1089/ten.tea.2018.0142.

35. J. K. Sahoo, J. Choi, O. Hasturk, et al., "Silk Degumming Time Controls Horseradish Peroxidase-Catalyzed Hydrogel Properties," *Biomaterials Science* 8 (2020): 4176–4185, https://doi.org/10.1039/D0BM00512F.

36. C. A. Werlang, J. K. Sahoo, G. Cárcarmo-Oyarce, et al., "Selective Biofilm Inhibition Through Mucin-Inspired Engineering of Silk Glycopolymers," *Journal of the American Chemical Society* 146 (2024): 34661–34668, https://doi.org/10.1021/jacs.4c12945.

37. O. Hasturk, K. E. Jordan, J. Choi, and D. L. Kaplan, "Enzymatically Crosslinked Silk and Silk-Gelatin Hydrogels With Tunable Gelation Kinetics, Mechanical Properties and Bioactivity for Cell Culture and Encapsulation," *Biomaterials* 232 (2020): 119720, https://doi.org/10.1016/j.biomaterials.2019.119720.

38. K. Sabet-Bokati and K. Plucknett, "Water-Induced Failure in Polymer Coatings: Mechanisms, Impacts and Mitigation Strategies—A Comprehensive Review," *Polymer Degradation and Stability* 230 (2024): 111058, https://doi.org/10.1016/j.polymdegradstab.2024.111058.

39. S. J. Park, "Protein–Nanoparticle Interaction: Corona Formation and Conformational Changes in Proteins on Nanoparticles," *International Journal of Nanomedicine* 15 (2020): 5783–5802, https://doi.org/10.2147/IJN.S254808.

40. C. Li, C. Guo, V. Fitzpatrick, et al., "Design of Biodegradable, Implantable Devices Towards Clinical Translation," *Nature Reviews Materials* 5 (2020): 61–81, https://doi.org/10.1038/s41578-019-0150-z.

41. C. Guo, C. Li, and D. L. Kaplan, "Enzymatic Degradation of Bombyx mori Silk Materials: A Review," *Biomacromolecules* 21 (2020): 1678–1686, https://doi.org/10.1021/acs.biomac.0c00090.

42. T. P. Lozito, W. M. Jackson, L. J. Nesti, and R. S. Tuan, "Human Mesenchymal Stem Cells Generate a Distinct Pericellular Zone of MMP Activities via Binding of MMPs and Secretion of High Levels of TIMPs," *Matrix Biology* 34 (2014): 132–143, https://doi.org/10.1016/j.matbio.2013.10.003.

43. W. Li, T. Guan, X. Zhang, et al., "The Effect of Layer-by-Layer Assembly Coating on the Proliferation and Differentiation of Neural Stem Cells," *ACS Applied Materials & Interfaces* 7 (2015): 3018–3029, https://doi.org/10.1021/am504456t.

44. D. C. Kirouac, G. J. Madlambayan, M. Yu, E. A. Sykes, C. Ito, and P. W. Zandstra, "Cell–Cell Interaction Networks Regulate Blood Stem and Progenitor Cell Fate," *Molecular Systems Biology* 5 (2009): MSB200949, https://doi.org/10.1038/msb.2009.49.

45. J. Su, Y. Song, Z. Zhu, et al., "Cell–Cell Communication: New Insights and Clinical Implications," *Signal Transduction and Targeted Therapy* 9 (2024): 196, https://doi.org/10.1038/s41392-024-01888-z.

46. S. Xiao, W. Stacklies, M. Cetinkaya, B. Markert, and F. Gräter, "Mechanical Response of Silk Crystalline Units From Force-Distribution

Analysis," *Biophysical Journal* 96 (2009): 3997–4005, https://doi.org/10.1016/j.bpj.2009.02.052.

47. M. Bao, J. Xie, N. Katoele, et al., "Cellular Volume and Matrix Stiffness Direct Stem Cell Behavior in a 3D Microniche," *ACS Applied Materials & Interfaces* 11 (2019): 1754–1759, https://doi.org/10.1021/acsami.8b19396.

48. M. Guo, A. F. Pegoraro, A. Mao, et al., "Cell Volume Change Through Water Efflux Impacts Cell Stiffness and Stem Cell Fate," *Proceedings of the National Academy of Sciences* 114 (2017): E8618–E8627.

49. T. Oki, K. Nishimura, J. Kitaura, et al., "A Novel Cell-Cycle-Indicator, mVenus-p27K−, Identifies Quiescent Cells and Visualizes G0–G1 Transition," *Scientific Reports* 4 (2014): 4012, https://doi.org/10.1038/srep04012.

50. P. Moreno-Layseca and C. H. Streuli, "Signalling Pathways Linking Integrins With Cell Cycle Progression," *Matrix Biology* 34 (2014): 144–153, https://doi.org/10.1016/j.matbio.2013.10.011.

51. M. Rumman, A. Majumder, L. Harkness, et al., "Induction of Quiescence (G0) in Bone Marrow Stromal Stem Cells Enhances Their Stem Cell Characteristics," *Stem Cell Research* 30 (2018): 69–80, https://doi.org/10.1016/j.scr.2018.05.010.

52. S. Murab, S. Chameettachal, M. Bhattacharjee, S. Das, D. L. Kaplan, and S. Ghosh, "Matrix-Embedded Cytokines to Simulate Osteoarthritis-Like Cartilage Microenvironments," *Tissue Engineering Part A* 19 (2013): 1733–1753, https://doi.org/10.1089/ten.tea.2012.0385.

53. J. A. Buckwalter, H. J. Mankin, and A. J. Grodzinsky, "Articular Cartilage and Osteoarthritis," *Instructional Course Lectures* 54 (2005): 465.

54. L. Liu, P. Luo, M. Yang, J. Wang, W. Hou, and P. Xu, "The Role of Oxidative Stress in the Development of Knee Osteoarthritis: A Comprehensive Research Review," *Frontiers in Molecular Biosciences* 9 (2022): 1001212, https://doi.org/10.3389/fmolb.2022.1001212.

55. J. Biddlestone, D. Bandarra, and S. Rocha, "The Role of Hypoxia in Inflammatory Disease (Review)," *International Journal of Molecular Medicine* 35 (2015): 859–869, https://doi.org/10.3892/ijmm.2015.2079.

56. K. Z. Juhász, T. Hajdú, P. Kovács, J. Vágó, C. Matta, and R. Takács, "Hypoxic Conditions Modulate Chondrogenesis Through the Circadian Clock: The Role of Hypoxia-Inducible Factor-1α," *Cells* 13 (2024): 512, https://doi.org/10.3390/cells13060512.

57. J. Shang, H. Liu, J. Li, and Y. Zhou, "Roles of Hypoxia During the Chondrogenic Differentiation of Mesenchymal Stem Cells," *Current Stem Cell Research & Therapy* 9 (2014): 141–147, https://doi.org/10.2174/1574888X09666131230142459.

58. B. Kacprzak and M. Stańczak, "Knee Joint Response to Mechanical Loading: Bounding Mechanotransduction with Rehabilitation," *Cellular Physiology and Biochemistry* 59 (2024): 666–729.

59. F. Maier, H. Drissi, and D. M. Pierce, "Shear Deformations of Human Articular Cartilage: Certain Mechanical Anisotropies Apparent at Large But Not Small Shear Strains," *Journal of the Mechanical Behavior of Biomedical Materials* 65 (2017): 53–65, https://doi.org/10.1016/j.jmbbm.2016.08.012.

60. Y. Wu, A. Li, N. Sun, et al., "Unveiling the Mechanisms of Mechanical Loading-Induced Knee Osteoarthritis Through Transcriptomics," *International Immunopharmacology* 157 (2025): 114785, https://doi.org/10.1016/j.intimp.2025.114785.

61. Y. Chisti, "Hydrodynamic Damage to Animal Cells," *Critical Reviews in Biotechnology* 21 (2001): 67–110, https://doi.org/10.1080/20013891081692.

62. S. Stolberg and K. E. McCloskey, "Can Shear Stress Direct Stem Cell Fate?," *Biotechnology Progress* 25 (2009): 10–19, https://doi.org/10.1002/btpr.124.

63. M. Grellier, R. Bareille, C. Bourget, and J. Amédée, "Responsiveness of Human Bone Marrow Stromal Cells to Shear Stress," *Journal of Tissue Engineering and Regenerative Medicine* 3 (2009): 302–309, https://doi.org/10.1002/term.166.

64. B. A. Aguado, W. Mulyasasmita, J. Su, K. J. Lampe, and S. C. Heilshorn, "Improving Viability of Stem Cells During Syringe Needle Flow Through the Design of Hydrogel Cell Carriers," *Tissue Engineering Part A* 18 (2012): 806–815, https://doi.org/10.1089/ten.tea.2011.0391.

65. S. Chawla, S. Midha, A. Sharma, and S. Ghosh, "Silk-Based Bioinks for 3D Bioprinting," *Advanced Healthcare Materials* 7 (2018): 1701204, https://doi.org/10.1002/adhm.201701204.

66. C. Sobajo, F. Behzad, X.-F. Yuan, and A. Bayat, "Silk: A Potential Medium for Tissue Engineering," *Eplasty* 8 (2008): 47.

67. J. Sapudom, M. Kongsema, and A. Methachittipan, "Degradation Products of Crosslinked Silk Fibroin Scaffolds Modulate the Immune Response But Not Cell Toxicity," *Journal of Materials Chemistry B* 11 (2023): 3607–3616, https://doi.org/10.1039/D3TB00097D.

68. M. Bhattacharjee, E. Schultz-Thater, E. Trella, et al., "The Role of 3D Structure and Protein Conformation on the Innate and Adaptive Immune Responses to Silk-Based Biomaterials," *Biomaterials* 34 (2013): 8161–8171, https://doi.org/10.1016/j.biomaterials.2013.07.018.

69. N. Majumder, M. Bhattacharjee, G. C. Spagnoli, and S. Ghosh, "Immune Response Profiles Induced by Silk-Based Biomaterials: A Journey From 'Immunogenicity' Towards 'Immuno-Compatibility'," *Journal of Materials Chemistry B* 12 (2024): 9508–9523, https://doi.org/10.1039/D4TB01231C.

70. P. Broz and V. M. Dixit, "Inflammasomes: Mechanism of Assembly, Regulation and Signalling," *Nature Reviews Immunology* 16 (2016): 407–420, https://doi.org/10.1038/nri.2016.58.

71. M. Singh, S. Kumar, B. Singh, et al., "The 1, 2-Ethylenediamine SQ109 Protects Against Tuberculosis by Promoting M1 Macrophage Polarization Through the p38 MAPK Pathway," *Communications Biology* 5 (2022): 759, https://doi.org/10.1038/s42003-022-03693-2.

72. C. Rosales and E. Uribe-Querol, "Phagocytosis: A Fundamental Process in Immunity," *BioMed Research International* 2017 (2017): 1–18, https://doi.org/10.1155/2017/9042851.

73. A. J. Knights, S. J. Redding, and T. Maerz, "Inflammation in Osteoarthritis: The Latest Progress and Ongoing Challenges," *Current Opinion in Rheumatology* 35 (2023): 128–134, https://doi.org/10.1097/BOR.0000000000000923.

74. F. Berenbaum, "Osteoarthritis as an Inflammatory Disease (Osteoarthritis is not Osteoarthrosis!)," *Osteoarthritis and Cartilage* 21 (2013): 16–21, https://doi.org/10.1016/j.joca.2012.11.012.

75. N. Majumder and S. Ghosh, "Unfolding the Mystery Behind the Onset of Chondrocyte Hypertrophy During Chondrogenesis: Toward Designing Advanced Permanent Cartilage-mimetic Biomaterials," *Advanced Functional Materials* 33 (2023): 2300651, https://doi.org/10.1002/adfm.202300651.

76. J. D. McCall, J. E. Luoma, and K. S. Anseth, "Covalently Tethered Transforming Growth Factor Beta in PEG Hydrogels Promotes Chondrogenic Differentiation of Encapsulated Human Mesenchymal Stem Cells," *Drug Delivery and Translational Research* 2 (2012): 305–312, https://doi.org/10.1007/s13346-012-0090-2.

77. S. Chawla, A. Mainardi, N. Majumder, et al., "Chondrocyte Hypertrophy in Osteoarthritis: Mechanistic Studies and Models for the Identification of New Therapeutic Strategies," *Cells* 11 (2022): 4034, https://doi.org/10.3390/cells11244034.

78. L. Kong, "Current Study and Novel Understanding for Macrophages," *Current Stem Cell Research & Therapy* 15 (2020): 557–558, https://doi.org/10.2174/1574888X1507200810094100.

79. Y. Chen, W. Jiang, H. Yong, et al., "Macrophages in Osteoarthritis: Pathophysiology and Therapeutics," *American journal of Translational Research* 12 (2020): 261.

80. Z. Yuan, D. Jiang, M. Yang, et al., "Emerging Roles of Macrophage Polarization in Osteoarthritis: Mechanisms and Therapeutic Strategies," *Orthopaedic Surgery* 16 (2024): 532–550, https://doi.org/10.1111/os.13993.

81. Y. Chen, W. Jiang, H. Yong, et al., "Macrophages in Osteoarthritis: Pathophysiology and Therapeutics," *American journal of Translational Research* 12 (2020): 261.

82. W. Zhang, M. Luo, Y. Xing, et al., "M2 Macrophage-Derived Extracellular Vehicles-Loaded Hyaluronic Acid-Alginate Hydrogel for Treatment of Osteoarthritis," *Orthopaedic Surgery* 17 (2025): 1867–1881.

83. A. Turkiewicz, Y. Díaz, J. L. Poveda-Marina, T. Duarte-Salles, and D. Prieto-Alhambra, "Knee Osteoarthritis and Risk of Ten Cancers in a Large Real-World Matched Cohort Study," *Osteoarthritis and Cartilage* 28 (2020): S421–S422, https://doi.org/10.1016/j.joca.2020.02.654.

84. C. Y. J. Wenham and P. G. Conaghan, "The Role of Synovitis in Osteoarthritis," *Therapeutic Advances in Musculoskeletal Disease* 2 (2010): 349–359, https://doi.org/10.1177/1759720X10378373.

85. A. Damerau, E. Rosenow, D. Alkhoury, F. Buttgereit, and T. Gaber, "Fibrotic Pathways and Fibroblast-Like Synoviocyte Phenotypes in Osteoarthritis," *Frontiers in immunology* 15 (2024): 1385006.

86. L. Zhang, R. Xing, and Z. Huang, "Synovial Fibrosis Involvement in Osteoarthritis," *Frontiers in Medicine* 8 (2021): 684389, https://doi.org/10.3389/fmed.2021.684389.

87. S. Chen, A. F. U. H. Saeed, Q. Liu, et al., "Macrophages in Immunoregulation and Therapeutics," *Signal Transduction and Targeted Therapy* 8 (2023): 207, https://doi.org/10.1038/s41392-023-01452-1.

88. S. El Harane, S. Durual, T. Braschler, et al., "Adipose-Derived Stem Cell Spheroids are Superior to Single-Cell Suspensions to Improve Fat Autograft Long-Term Survival," *Journal of Cellular and Molecular Medicine* 26 (2022): 1421–1433, https://doi.org/10.1111/jcmm.17082.

89. H. Shen, S. Cai, C. Wu, W. Yang, H. Yu, and L. Liu, "Recent Advances in Three-Dimensional Multicellular Spheroid Culture and Future Development," *Micromachines* 12 (2021): 96.

90. Y. Li, W. Luo, S. A. Zhu, and G. H. Lei, "Gene-Specific Substitution Profiles Describe the Types and Frequencies of Amino Acid Changes During Antibody Somatic Hypermutation," *Frontiers in Immunology* 8 (2017): 356, https://doi.org/10.3389/fimmu.2017.00537.

91. C. L. Wu, N. S. Harasymowicz, M. A. Klimak, K. H. Collins, and F. Guilak, "The Role of Macrophages in Osteoarthritis and Cartilage Repair," *Osteoarthritis and Cartilage* 28 (2020): 544–554, https://doi.org/10.1016/j.joca.2019.12.007.

92. M. McGill, J. M. Coburn, B. P. Partlow, X. Mu, and D. L. Kaplan, "Molecular and Macro-Scale Analysis of Enzyme-Crosslinked Silk Hydrogels for Rational Biomaterial Design," *Acta Biomaterialia* 63 (2017): 76–84, https://doi.org/10.1016/j.actbio.2017.09.020.

93. L. Sun, S. Zhang, J. Zhang, N. Wang, W. Liu, and W. Wang, "Fenton Reaction-Initiated Formation of Biocompatible Injectable Hydrogels for Cell Encapsulation," *Journal of Materials Chemistry B* 1 (2013): 3932–3939, https://doi.org/10.1039/c3tb20553c.

94. L. S. Moreira Teixeira, J. Feijen, C. A. van Blitterswijk, P. J. Dijkstra, and M. Karperien, "Enzyme-Catalyzed Crosslinkable Hydrogels: Emerging Strategies for Tissue Engineering," *Biomaterials* 33 (2012): 1281–1290, https://doi.org/10.1016/j.biomaterials.2011.10.067.

95. S. W. Ryter, P. K. Hong, and A. Hoetzel, "Mechanisms of Cell Death in Oxidative Stress," *Antioxidants & Redox Signaling* 9 (2007): 49–89, https://doi.org/10.1089/ars.2007.9.49.

96. T. Chidawanyika and S. Supattapone, "Hydrogen Peroxide-Induced Cell Death in Mammalian Cells," *Journal of Cellular Signaling* 2 (2021): 206.

97. N. E. Ryu, S. H. Lee, and H. Park, "Spheroid Culture System Methods and Applications for Mesenchymal Stem Cells," *Cells* 8 (2019): 1620, https://doi.org/10.3390/cells8121620.

98. C. Johnbosco, M. Becker, N. Willemen, et al., "Covalent On-Cell Conjugation of Biomaterials Through Oxidative Phenolic Coupling Regulates Stem Cell Fate via Intracellular Biophysical Programming," *Advanced Functional Materials* 35 (2025): 2418963, https://doi.org/10.1002/adfm.202418963.

Supporting Information

Additional supporting information can be found online in the Supporting Information section.

Supporting File: smll73772-sup-0001-SuppMat.docx.